DEVELOPMENT OF AN OPTICAL SUPERHETERODYNE RECEIVER

INTERIM FINAL REPORT NO. 2

March 1965 - October 1966

R. Lucy

NASA Contract NAS8-11588

Submitted to

GEORGE C. MARSHALL SPACE FLIGHT CENTER
Huntsville, Alabama

APPLIED RESEARCH LABORATORY
SYLVANIA ELECTRONIC SYSTEMS
A Division of Sylvania Electric Products Inc.
40 SYLVAN ROAD, WALTHAM, MASSACHUSETTS 02154

DEVELOPMENT OF AN OPTICAL SUPERHETERODYNE RECEIVER

INTERIM FINAL REPORT NO. 2

March 1965 - October 1966

R. Lucy

~~NASA~~ Contract NAS8-11588

Submitted to

GEORGE C. MARSHALL SPACE FLIGHT CENTER
Huntsville, Alabama

APPLIED RESEARCH LABORATORY
SYLVANIA ELECTRONIC SYSTEMS
A Division of Sylvania Electric Products Inc.
40 SYLVAN ROAD, WALTHAM, MASSACHUSETTS 02154

TABLE OF CONTENTS

TABLE OF CONTENTS - Continued

LIST OF ILLUSTRATIONS

PART 1

OPTICAL SUPERHETERODYNE RECEIVER

1.1 INTRODUCTION

An operational model of the optical superheterodyne receiver, completely analogous to a radio frequency receiver, has been designed, constructed, and tested for NASA by the Applied Research Laboratory of Sylvania Electronic Systems, a Division of Sylvania Electric Products Inc. The receiver, which operates at 6328 Å and is mounted in a mobile van, can coherently detect signals from a remote laser transmitter. The receiver is immediately applicable to both coherent and noncoherent communications experiments from air to ground or space to ground, including the proposed Laser Communications Satellite Experiment of the Apollo Applications Program.

Included in the receiver are facilities for:

1) An automatic frequency control system that allows the local oscillator of the receiver to automatically track the transmitter frequency over a 1-GHz Doppler frequency range.

2) An automatic angle tracking servo system that allows the receiver to track a satellite-borne transmitter moving at angular rates as high as 4 milliradians/second with an rms accuracy of 25 microradians.

3) Amplitude and frequency modulation detection of television bandwidth information signals imposed upon the optical carrier at the transmitter.

Figure 1 is a block diagram of the receiver. Figure 2 shows the physical structure of the optics and the associated phototubes of the receiver and Figure 3 shows the electronics portion of the receiver.

This equipment, the first prototype of an operational coherent laser communications system to emerge from the laboratory, has been used in series of communications experiments.

The communications experiments, designed to evaluate the Optical Superheterodyne Receiver and also compare coherent and noncoherent optical detector techniques, have resulted in obtaining typical fading data for the above-mentioned techniques. The experiments were performed over a 1-kilometer path,

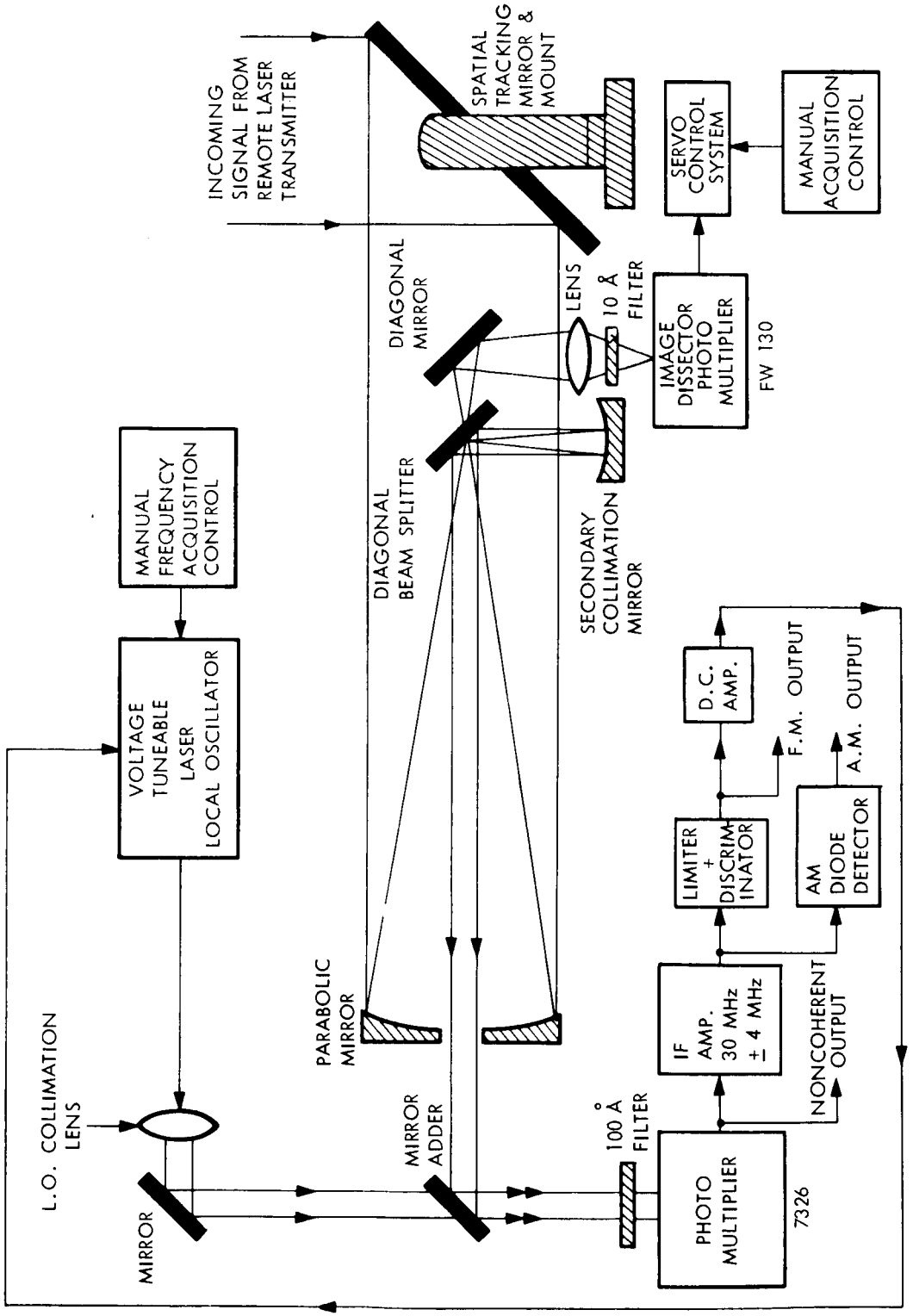

Figure-1. Optical Superheterodyne Receiver

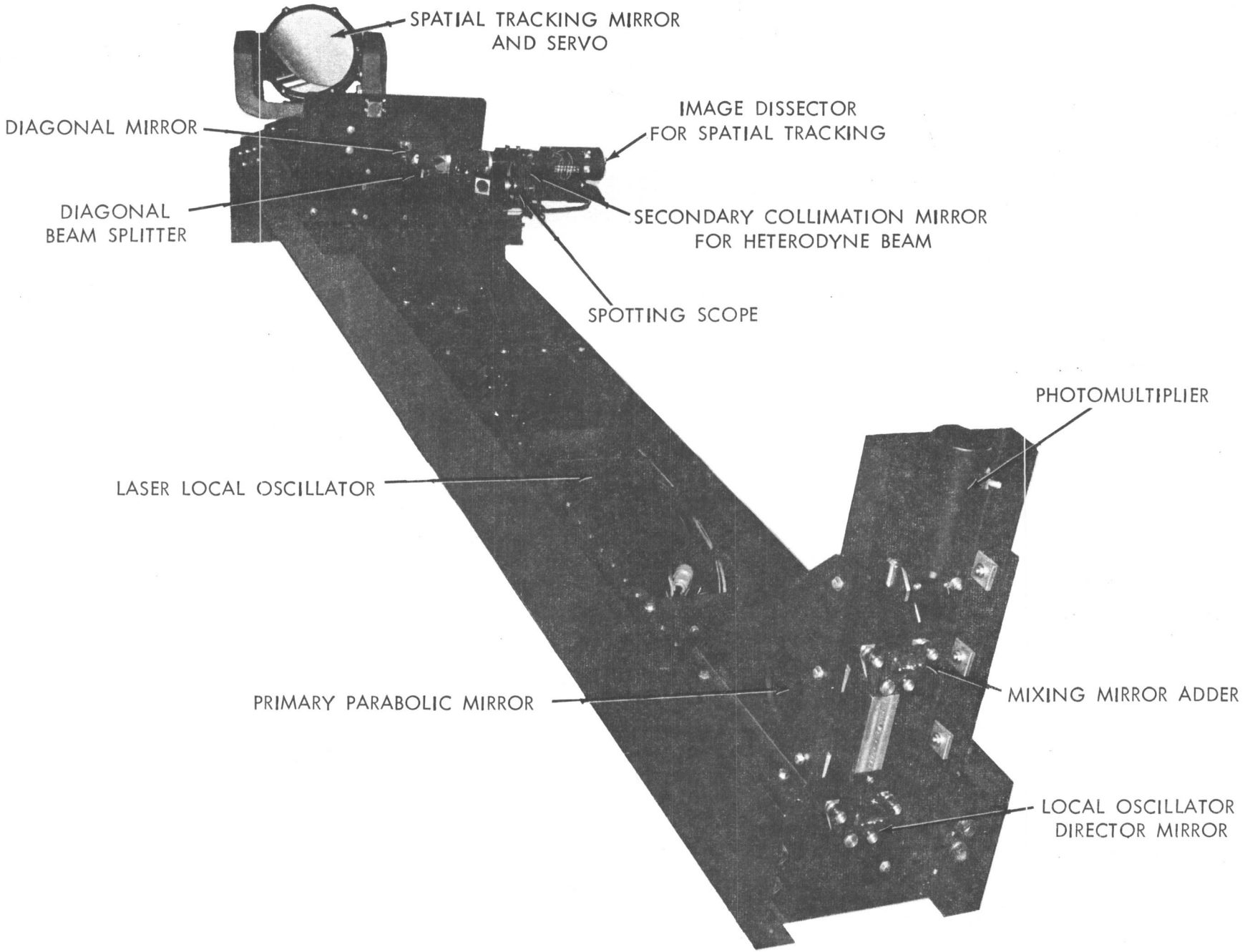

Figure 2. Optical Superheterodyne Receiver Optics

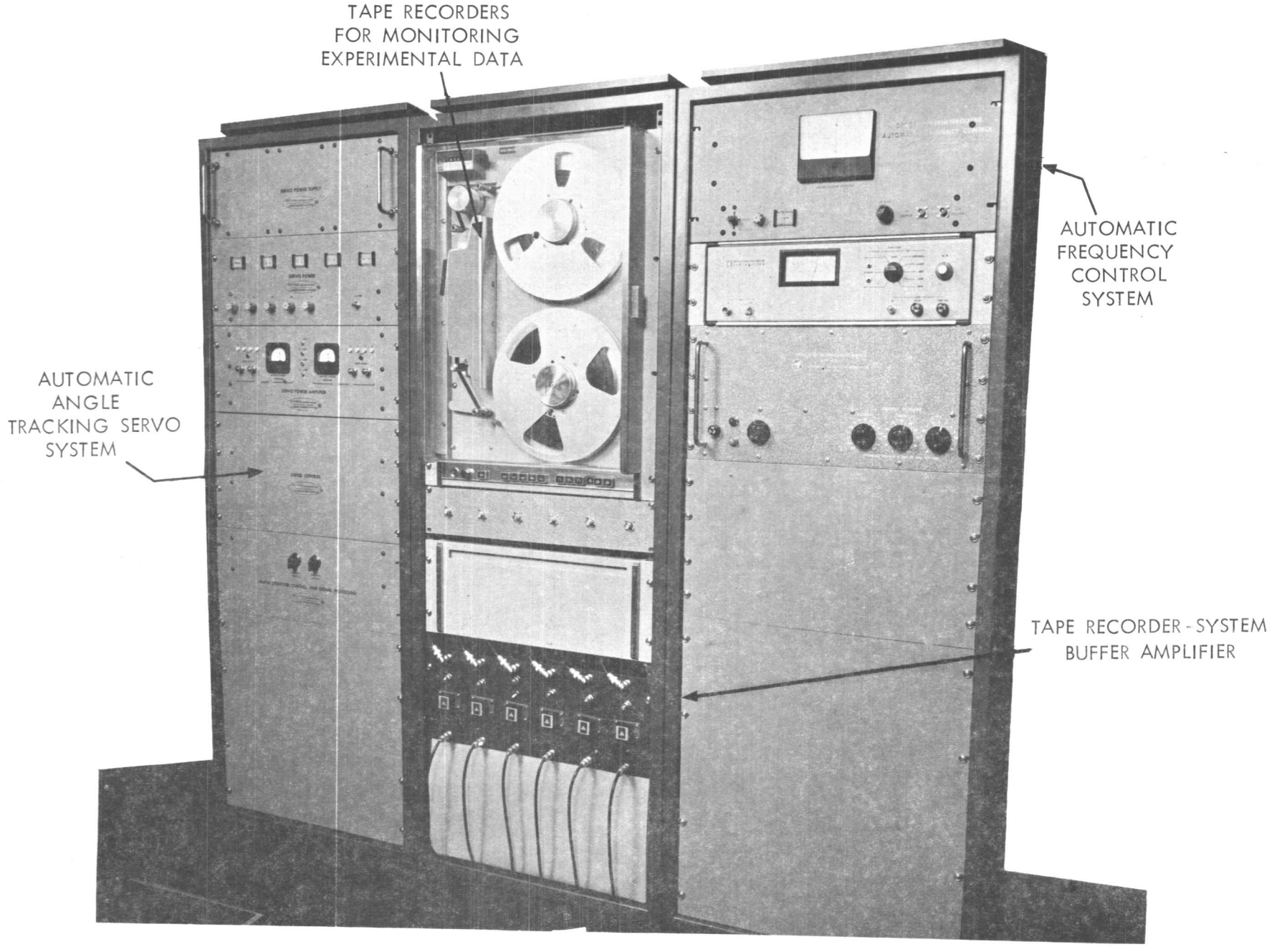

Figure 3. System Electronics

using a remote laser transmitter and the optical superheterodyne as a receiver. Both long and short-term results have been obtained. These data, plus results of frequency modulation experiments, provide information for the comparison of a noncoherent amplitude modulation system, a coherent amplitude modulated system, and a coherent frequency modulated system. In general, the present results show the superiority of noncoherent detection techniques when the system is not limited by background radiation noise. In the future, we expect the coherent performance to be improved, the extent of which is not now known.

1.2 OPTICAL SUPERHETERODYNE RECEIVER

1.2.1 General Description

A diagram of the optical superheterodyne receiver is shown in Figure 1. The superheterodyne optics, a Mersenne telescope,[1] consists of two concave, confocal paraboloidal reflectors. The received rays are reflected from the tracking mirror to the primary parabolic mirror and thence to the secondary beam-forming parabola. The signal is then mixed with the local signal at the mirror adder and the resultant beat detected by the photomultiplier.

The receiver uses a precision angle tracking servo-controlled mirror[2] to maintain alignment between the incoming signal and the receiver telescope. Another optical signal takeoff provides angular data to an image dissector photomultiplier to control the tracking mirror.

The beat-frequency output of the photomultiplier is fed to a 30-MHz, $\pm$4-MHz intermediate frequency amplifier and thence to a limiter-discriminator combination. The low-frequency output of the discriminator output is amplified and used to control the local oscillator to provide automatic frequency control. The local oscillator is a voltage-tuned Spectra Physics, Inc. Model

1. King, Henry C. The History of the Telescope, Sky Publishing Corp., Cambridge, Massachusetts, 1959.

2. R. F. Lucy, C. J. Peters, E. J. McGann, and K. T. Lang, "Precision Laser Automatic Tracking System," Applied Optics, vol. 5, pp. 517-524; April 1966.

119 single-frequency laser. Initial search and frequency acquisition is performed manually. An FM and AM coherent signal output is provided in addition to a noncoherent output to measure optical power. Interference type optical filters are used in front of both the receiver and tracking detectors.

The receiver optics are shown in Figure 2 and the electronics are shown in Figure 3. In addition to the necessary electronics, a multichannel tape recorder with buffer amplifiers to record signal data during experiments is also shown.

1.2.2 Optics

The primary mirror of the Mersenne telescope is a 2.44-meter focal length, 20.3-cm diameter paraboloid figured to an accuracy of 1/50 wavelength. The secondary mirror is an 18.8-cm focal length, 7.6-cm diameter paraboloid also figured to an accuracy of 1/50 wavelength. The ray budle converging from the primary to the common focus subtends 83.5 milliradians and only fills a 1.57-cm diameter area at the secondary collimation mirror. The local oscillator collimation lens is approximately an f/75, 1.15-meter focal length lens.

In order to increase the sensitivity of the optical heterodyne receiver, the optics are designed to intercept and collect as much energy as possible. A somewhat different set of rules is required for the design of such a collecting system as compared to ordinary telescope mirror design. In telescope design the goal is to focus all the energy from an object point to a corresponding point in the image plane. Point to point image phase relationships are not a primary consideration. In the optics for an optical heterodyne receiver the phase relationships are of the utmost importance. The main goal is to coherently add the signal collected from a coherent source with a local oscillator and produce a maximum heterodyne signal.

A turbulent atmosphere containing air blobs of different index of refraction can produce angular deviations of the propagated beam in its entirety or in part. The size of the atmospheric blobs or turbulons, as compared to the beam size, determines whether the beam line of sight is deviated or whether the beam is internally disrupted.

Angular fluctuations of the input signal produce angular misalignments between the signal and the local oscillator that will, in turn, produce heterodyne signal fading effects. If the entire wavefront at the aperture input is tilted, then the spatial tracking mirror provides a means of eliminating the variations that are within the 30-Hz response and ±25 microradian rms tracking accuracy limits of the servo.

Angular fluctuations can occur at higher frequencies. In addition, the received beam can be composed of many groups of rays of different angular tilts caused by individual refractions within the beam. In this case the servo would only track the centroid. Furthermore, angular fluctuations smaller than those correctable by the servo will still produce a severe effect on the receiver performance.

An operational heterodyne receiver must be capable of operating over varying ranges and through a turbulent atmosphere. Consequently the optics must be designed to cope with these variable conditions. As with all operating systems, compromises must be made. These tradeoffs inevitably reduce the efficiency of operation. In the design of the optical superheterodyne receiver reduced sensitivity has been accepted to provide a design that will be less sensitive to angular fluctuations between the signal and local oscillator. In addition, this design is compatible with both near and far field conditions of a receiver-transmitter combination.

1.2.2.1 Near Field--Far Field Considerations

By utilizing a spherical mixing geometry, the heterodyne receiver optics can be adjusted to operate the receiver in the near field with large apertures as well as the far field. When the receiver is in the far field (Fraunhofer region) of the transmitter, the signal at the receiver aperture is essentially a plane wave. When the Mersenne telescope is adjusted for the confocal condition and the atmospheric effects are negligible, the collimated output wave from the smaller secondary mirror is also a plane wave.[3]

3. E. H. Linfoot, Recent Advances in Optics, Oxford University Press, London, p. 277; 1958.

If the atmosphere perturbs the wavefront, then the corresponding perturbations appear in the output beam magnified by the ratio of the primary to secondary focal length. As the distance between a point source transmitter and receiver is decreased, the receiver enters the near field (Fresnel region) of the transmitter and a constant phase front at the receiver aperture is spherical. When a paraboloid is illuminated by a spherical wave all the rays over the aperture do not converge to a common point. Thus, it would be impossible to collimate these rays into a parallel beam with these optics. For a point source object and the confocal condition, all the rays reflected from the secondary parabola diverge with a curvature that is approximately the primary to secondary focal length ratio times the curvature of the input wave. Consequently, for fixed confocal paraboloids, the local oscillator wavefront would be adjusted for the best wavefront match between the two signals.

Certainly for near field situations, the Mersenne telescope alters the uniformity of the input wave because of the aforementioned aberration. However, it should be remembered that the purpose of this optical system is not to achieve perfect heterodyning but only to develop a compromise situation that will minimize complete signal fading due to destructive interference effects. We have found that a compromise can be achieved by utilizing a mixing geometry in which the local oscillator and received signal wavefronts are waves of different curvature.

1.2.2.2 Photomixing with Misaligned Wavefronts

The directional properties of optical heterodyne receivers are well known.[4] The wavefronts of the optical signal must be perfectly matched to the wavefront of the local oscillator to obtain a maximum efficiency. If the wavefronts are inclined to each other, the photocurrent signal can be severely degraded. An example of the requirement is found in interferometers in which interference fringes are produced as a result of one wavefront being at a slight angle with the other. In the typical interferometers, two waves of the

4. A. E. Siegman, "The Antenna Properties of Optical Heterodyne Receivers," Applied Optics, vol. 5, no. 10, pp. 1588-1594; October 1966.

same frequency are used to produce the interference pattern. In our case the waves are at slightly different frequencies; thus, there is a heterodyne beat between the two wavefronts. If we could observe the area of interference we would see the interference pattern changing with time. The bright and dark bands (areas of apposite phases) would move in progression across the observation area at the beat frequency rate. The changing pattern is indicative of the changing phases between the two optical waves of different frequencies.

If a phototube surface were illuminated with this pattern then the cross section of the photocurrent output would be a replica of the time-changing interference pattern. The AC component of the photocurrent would be the beat frequency. The DC component would be proportional to the intensities of the two optical waves. The anode of the phototube sums the instantaneous values of all the signals. If there are many fringes in the pattern, the alternate plus and minus signal components cancel each other. The net photocurrent would be the residual after the cancellation. For example, using the interferometer analogy, if there are 6 bright and 5 dark fringes at any instant of time, then 5 fringes of one polarity of phases cancel 5 fringes of the other polarity and only 1/11 of the total AC signal remains. As the number of fringes is decreased by better matching of the wavefronts, then the AC beat component collected by the anode increases.

If the angular misalignment varies in time the number of fringes varies accordingly. If there are an equal number of regions of opposite phases then the residue of uncancelled components can drop to zero. In a communication system complete signal dropouts (100 percent fading) is undesirable.

For a fixed fringe pattern apertures could be placed over areas representing one phase polarity to prevent cancellation effects. However, the turbulent atmosphere produces unknown angular changes and wavefront distortions of the received signal, and the design of an aperture to provide an optimum spatial filter is not known.

In order to provide the optical superheterodyne receiver with a means of operating without complete fading in a turbulent atmosphere and also provide both near and far field operation, a mixing geometry in which waves of

different curvature are employed was arrived at. A series of fringe experiments using the receiver optics shows the technique.

In order to introduce a plane wave into the receiver optics, a diffraction-limited 48-meter focal length, 15-cm diameter parabolic mirror was used to collimate a portion of the local oscillator laser. The nearly parallel beam was fed through the heterodyne system optics and allowed to form an interference pattern with the remaining portion of the laser local oscillator directly at the film plane of a 16-mm camera. Nearly plane wave fringing is shown in Figures 4a and 4b. In Figure 4a, the local oscillator and received signal are colinear. In Figure 4b there is a 70 microradian angle between the local oscillator signal and the received signal. The alternate light and dark bands of fringes represent a continuously varying phase between the local oscillator and received signal. If the amplitude of the fringes were summed, the signal in the bright band cancels the signal in a dark band. In the most severe misaligned case where there are many more light and dark bands, the uncancelled residue is small implying that the analogous photomixing process would be inefficient. In addition, summed output drops to zero when there are equal light and dark areas and rises to a local small maximum when there is an excess of one kind or the other. Consequently small angular disturbances can produce a 100 percent modulation on the summed signal. Jitter in the servo or optical signal angle of arrival fluctuations caused by atmospheric turbulence will thus produce a noise modulation of the signal. In the example of Figure 4a and 4b an angular change at the optics input of about 2.3 microradians changes the analogous mixing efficiency from a maximum to a minimum.

In Figure 4c two spherical waves of different curvature are perfectly aligned to produce a circular fringe zone pattern similar to Newton's Rings. Since the area of each zone is the same, the integrated value would be zero if there are an equal number of zones of alternate phases. However, as the angle between the two wavefronts is changed an asymmetrical pattern is produced as shown in Figure 4d. By using a square aperture and the nonsymmetrical behavior with wavefront misalignment, a nonzeroing mixing function has been apparently achieved over limited angular misalignments.

(a)

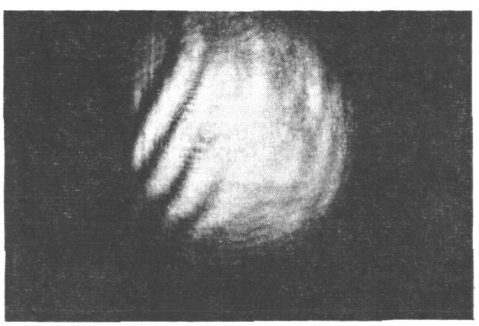

TWO PLANE WAVES NEARLY
COLLIMATED

(b)

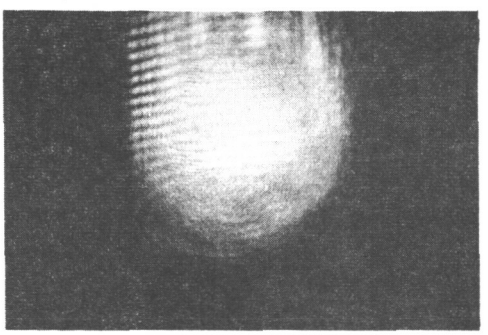

TWO PLANE WAVES
70 MICRO RADIANS TILT

(c)

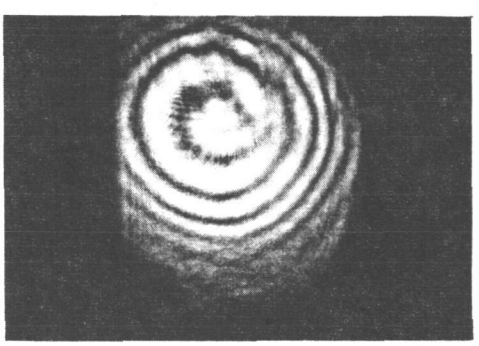

TWO SPHERICAL WAVES
400 CM RADIUS OF CURVATURE
1600 CM RADIUS OF CURVATURE
(COLLINEAR)

(d)

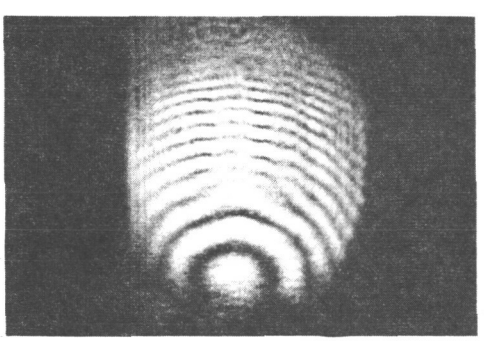

TWO SPHERICAL WAVES
400 CM RADIUS OF CURVATURE
1600 CM RADIUS OF CURVATURE
70 MICRO RADIUS TILT

Figure 4. Optical Mixing Experiments

Experiments performed on the operating system have shown that although the mixing efficiency is only a few percent, this technique of mixing does not null over ±100 microradian angular changes at the input to the optics.

1.2.2.3 Angular Sensitivity of Parabolic Primary Mirror

An important consideration in the optics design is the overall alignment accuracy required between the servo control system and heterodyne primary optics. If the parabola is tilted with respect to an incoming plane wave, then a comatic off-axis focus is formed. In order to determine the phase degradation across the focal plane, the focal plane phase of all the ray paths with respect to a plane wave input was calculated was a function of the angle of tilt of a paraboloid on a GE225 computer. The contributions from each incremental parabolic area were summed vectorially over the coma image. The resultant value was thus proportional to the net heterodyne signal power. Figure 5 shows the result of this calculation.

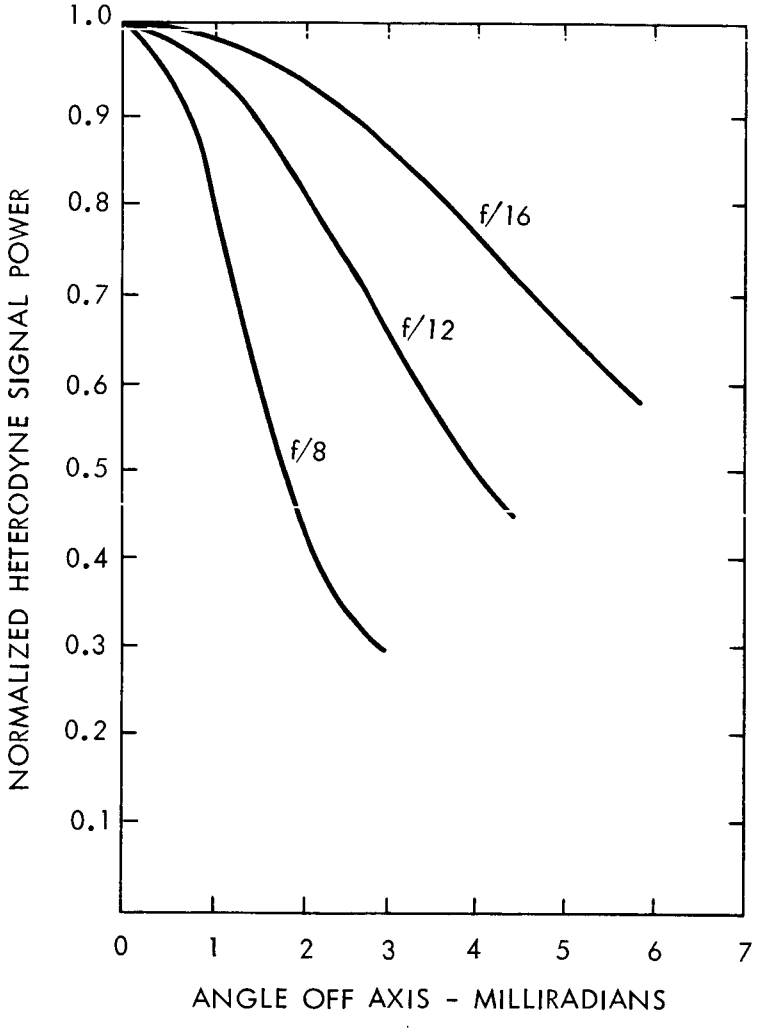

Figure 5. Angular Sensitivity Of Primary Paraboloid Mirror.

To verify the calculation the optics were tested at an f/20 aperture ratio during heterodyning experiments. It was found that heterodyning was not impaired over input angle of arrival variations of up to 100 microradians providing local oscillator and signal alignment were readjusted to accommodate the input angular offset. Without readjustment the allowable offset increments were found to be only $\pm$100 microradians. This value determined the design requirements placed upon the angle tracking servo accuracy.

1.2.3 Photomixer

The optical superheterodyne receiver is signal photon noise limited.[5] The receiver, signal-to-noise ratio at the 7326 photomultiplier output is given by the voltage ratio

$$\frac{e_{so}}{e_{no}} = \epsilon_1 \sqrt{\frac{QP_s}{h\nu\Delta f}} \qquad (1)$$

where

ϵ_1 is the heterodyne efficiency

Q is the quantum efficiency

P_s is the signal power

$h\nu$ is the energy per photon

Δf is the electrical noise bandwidth.

In order to obtain photon noise limited operation the local oscillator level is adjusted to a value so that its photon noise predominates.[5] The sensitivity expressed by Equation (1) will be degraded if the amplification following the photosurface detection process introduces a noise power greater

5. G. Biernson and R. F. Lucy, "Requirements of a Coherent Laser Pulse Doppler Radar," Proc. IEEE, vol. 51, pp. 202-213; January 1963.

than $h\nu\Delta f/Q$. In photomultipliers the secondary emission amplification introduces some noise. This additional noise degrades the value of Equation (1) about 1 dB in standard box type multipliers. In photomultipliers this "noiseless" amplification is sufficiently large to eliminate further signal-to-noise degradation by the amplifiers following the tube output.

Standard fast rise time tubes have 3-dB cutoff frequencies of about a 100 MHz. In this system the detector bandwidth must only be greater than the IF bandwidth following the detection, even for Doppler frequency tracking to 1 GHz, because a tunable optical local oscillator is used.

1.2.4 Local Oscillator

The laser local oscillator noise and power requirements are discussed in Reference 5. Ideally, sufficient monochromatic power should be available to permit discrimination against random noise-producing sources, such as reflected or scattered sunlight. Also, the noise produced at the output of the photomixer due to the local oscillator should not exceed the expected shot noise level for the corresponding local oscillator power. A single frequency laser, the Spectra Physics Model 119 laser, has been evaluated for this purpose and found to be satisfactory. The monochromatic power output is approximately 100 μW. Anticipated severe background levels, such as a bright cloud, should not exceed 0.1 μW within the system.[5] Thus, if the local oscillator is 10 μW, then adequate background discrimination is provided. Measurements of the noise in a 4-MHz bandwidth for the laser used showed the noise to be uniformly distributed in frequency. The rms value of noise voltage from the photomixer exceeded by approximately three times the minimum shot noise level expected for this amount of optical power. This level degrades the system performance described in Equation (1).

The laser is voltage tunable over a 1200-MHz range at a rate up to 5 kHz, and is used in the frequency-tracking loop to cover a Doppler range of $\pm$500 MHz.

1.2.5 Doppler Frequency Tracking

The laser signal containing the Doppler shift is mixed with the optical local oscillator signal in the photomixer. The output of the photomixer con-

taining the Doppler frequency is fed into the 30 MHz $\pm$4 MHz IF amplifier. The IF amplifier has 84 dB of gain and a 6dB noise figure. The output is then fed into a limiter with 20 dB of quieting and thence to the discriminator.

In the closed-loop operation an error signal is developed at the discriminator which keeps the difference frequency between the two signals at a constant IF value.

The bandwidth of the AFC loop was chosen at the minimum value consistent with the expected rates of change of frequency to optimize the signal-to-noise ratio.

The AFC loop bandwidth is determined by the maximum rate-of-change of the input frequency expected. The maximum frequency deviation rate due to microphonic excitation of the Spectra Physics Model 119 has been found to be 10^8 Hz/s. The allowable design error was required to be half of the AFC loop bandwidth of $\Delta f_c/2$, thus the necessary loop bandwidth (gain-crossover frequency) is designed to be

$$\dot{f}\tau_c = \frac{\Delta f_c}{2} \tag{2}$$

where

$$\tau_c = \text{amplifier tune constant} = \frac{1}{2\pi \Delta f_c}$$

$$\dot{f} = 10^8 \text{ Hz/s}$$

$$\Delta f_c = 5.7 \times 10^3 \text{ Hz}$$

The bandwidth necessary to accommodate the rate of change of the received signal frequency due to relative motion between the system end points can be calculated in a similar manner. For a mission such as a missile being launched straight up from a launch pad at a certain distance from the receiver, the maximum rate-of-change of Doppler occurs at an elevation of $\pi/4$ radians and is proportional to the $\sqrt{2}$ times the missile acceleration. For a missile

undergoing an acceleration of 100 ft/s^2 the maximum Doppler rate of change is approximately 150 MHz/s. To track this rate of change in frequency on the incoming signal the bandwidth must be 6.7 kHz.

As in any tracking system the accuracy[2] with which the AFC loop can operate will be a function of the signal-to-noise ratio. The tracking error δf in the loop bandwidth Δf_c is approximately[2]

$$\delta f = \frac{\Delta f_e}{e_{so}/e_{no}} \tag{3}$$

A galvanometer at the discriminator output is used to indicate signal presence. Initial signal acquisition is performed by manually tuning the laser until the galvanometer deflection indicates the signal presence. When the meter nulls in the center of the discriminator curve, frequency control is manually switched to automatic. During prolonged system experiments lasting 14 hours, the AFC circuit has continually operated and kept the two remotely located lasers locked together.

1.2.6 Spatial Tracking

The spatial tracking function of the optical superheterodyne receiver is of vital importance to the receiver flexibility. The heterodyne optics and subsequent photomixing operation are extremely sensitive to angular changes of the signal direction. The spatial tracking follows the line-of-sight direction of transmitted signal and maintains the signal along the optical axis of the system. Tests performed upon the optical superheterodyne receiver have shown that the angular limits of operation are $\pm$ 100 microradians. Thus, the angular tracking accuracy of the spatial tracking system must be less than this value. The total error is the sum of the dynamic error arising from the relative motion between the receiver and the transmitter plus the static error produced by frictional torques and tachometer noise.

Extensive tests[2] on an identical earlier model of the tracking mirror have shown the folowing results. When tracking low acceleration targets such

as satellites and airplanes, this tracker has an accuracy of approximately 25 microradians rms. The accuracy under these conditions is set by the static friction and equivalent noise bandwidth of the tracker and the scintillation of the atmosphere. When tracking high acceleration targets such as rockets, this type of unit has a tracking error which is directly proportional to the angular acceleration of 0.6 radians/second^2; the tracking angular error peaks to 0.3 milliradians at launch and settles to 0.1 milliradian within 0.1 second thereafter. Thus, the tracking accuracy against low acceleration targets is comparable to the accuracy of a star tracker.

The angular error sensor is an image dissector operated noncoherently. Adequate background discrimination[5] is achieved by using a 10 $\mathring{A}$ optical filter and by virtue of the narrow-band response of the servo. The controlled member in the tracker is a two-axis gimballed mount on which is carried the flat tracking mirror. Both axes of this mount are powered by DC torque motors directly coupled to the unit. Angular rate feedback information is obtained by DC tachometers which are also fastened directly to their respective axes.

The lowest structural resonance occurs about the azimuth axis at 45 Hz. This resonance limits the azimuth gain crossover frequency but does not significantly affect the elevation loop. The rate loop gain crossover frequencies are 30 Hz in the azimuth and 50 Hz in the elevation channel. The position loop gain crossover frequencies are 10 Hz in azimuth and 17 Hz in elevation. Both axes have integral networks with an upper break frequency of 2 Hz and a lower break frequency at 0.02 Hz. The equivalent noise bandwidth for the tracker is 19 Hz in the azimuth and 30 Hz in the elevation.

High precision bearings of the ABEC class 7 type are used in both axes. Including the contributions from the various potentiometers, tachometers, and motors, the measured static friction on both axes is 7×10^{-2} ft-lb. The static pointing accuracy on both axes is on the order of 10 microradians.

1.3 GROUND-BASED COMMUNICATIONS EXPERIMENTS USING THE OPTICAL SUPERHETERODYNE RECEIVER

The effect of a turbulent atmosphere on the propagation of laser beams is well known.[6-14] Some of the previous work is experimental but the majority is theoretical. Very little of the available data is in a form that can be used to directly compare the performance of coherent and noncoherent detection techniques. In addition, no data is actually available for a fully operable coherent system. Consequently, a series of communications experiments to evaluate the optical superheterodyne receiver, operating in a real atmospheric environment, and to compare it to a noncoherent detection method were performed.

A remote laser transmitter consisting of a single-frequency 6328 Å laser, a Sylvania S-2-ϕ phase modulator, and beam-forming optics was mounted on a

6. I. Goldstein, P. A. Miles, and A. Chabot, "Heterodyne Measurements of Light Propagation Through Atmospheric Turbulence," Proc. IEEE, vol. 53, no. 9, pp. 1172-1180; September 1965.

7. P. Bechmann, "Signal Degeneration in Laser Beams Propagated Through a Turbulent Atmosphere," Radio Sci. J. Res., NBS/USNC-URSI, vol. 69D; April 1965.

8. S. Gardner, "Some Effects of Atmospheric Turbulence on Optical Heterodyne Communications," 1964 IEEE Internat'l Conv. Rec., pt. 6.

9. G. O. Reynolds and T. J. Skinner, "Mutual Coherence Function Applied to Imaging Through a Random Medium," J. Opt. Soc. Am., vol. 54, pp. 1302-1309; November 1964.

10. B. Cooper, "Optical Communication in the Earth's Atmosphere," IEEE Spectrum, pp. 83-88; July 1966.

11. H. Hodara, "Laser Wave Propagation Through the Atmosphere," Proc. IEEE, vol. 54, no. 3, pp. 368-375; March 1966.

12. J. I. Davis, "Consideration of Atmospheric Turbulence in Laser System Design," Applied Optics, vol. 5, no. 1, pp. 139-147; January 1966.

13. S. E. Miller and L. C. Tillotson, "Optical Transmission Research," Applied Optics, vol. 5, no. 10, pp. 1538-1549; October 1966.

14. R. F. Lucy, "The Effect of a Turbulent Atmosphere on a Coherent Laser System," 1964 NEREM Record.

rigid tripod-supported optical bench. The transmitter was located at a nominal distance of 1 km from the van-mounted optical superheterodyne receiver as shown in Figure 6. For these experiments the transmitter beamwidth exit size was approximately 1 cm-in diameter and then was optically spread to approximately 2 milliradians in order to reduce the effects of tripod and supporting structure vibration, thermostructural changes, and beam-line-of-sight fluctuations due to the atmosphere near the transmitter. With this relatively wide angle transmitter, we could easily point the transmitter and have it remain in position without attendance during an entire day of operation and testing. The signal power fading due to transmitter instabilities were thus reduced to less than 5 percent. Signal power fading due to the remainder of the atmospheric path averaged from 25 to 85 percent, depending upon meterological conditions. The fading depth of the heterodyne signal ranged all the way to complete momentary signal dropouts. Thus, line-of-sight variations effects were relatively small in comparison.

The optical superheterodyne receiver van was instrumented to record the data of the experiments. The instrumentation included a 7-channel tape recorder for short-term data and operational amplifiers to provide the necessary interface circuitry between the optical superheterodyne receiver outputs and the tape recorder.

The signal outputs simultaneously recorded included the received signal power, the heterodyne signal level, angle of arrival fluctuations as extracted from the azimuth and elevation spatial tracking servo-error signal, and the heterodyne signal frequency fluctuations as measured at the discriminator output. The instrumentation was thoroughly checked out and found to operate satisfactorily over a linear dynamic range of 30 to 1 and uniform bandwidth from DC up to frequencies large enough to cover the atmospheric fluctuation rate.

The experiments performed with the optical superheterodyne receiver have resulted in obtaining typical fading data on both noncoherent and coherent detection techniques for different atmospheric conditions over a 1 km atmospheric path. These data, plus results of frequency modulation experiments, provide the necessary information for the comparison of a noncoherent amplitude-

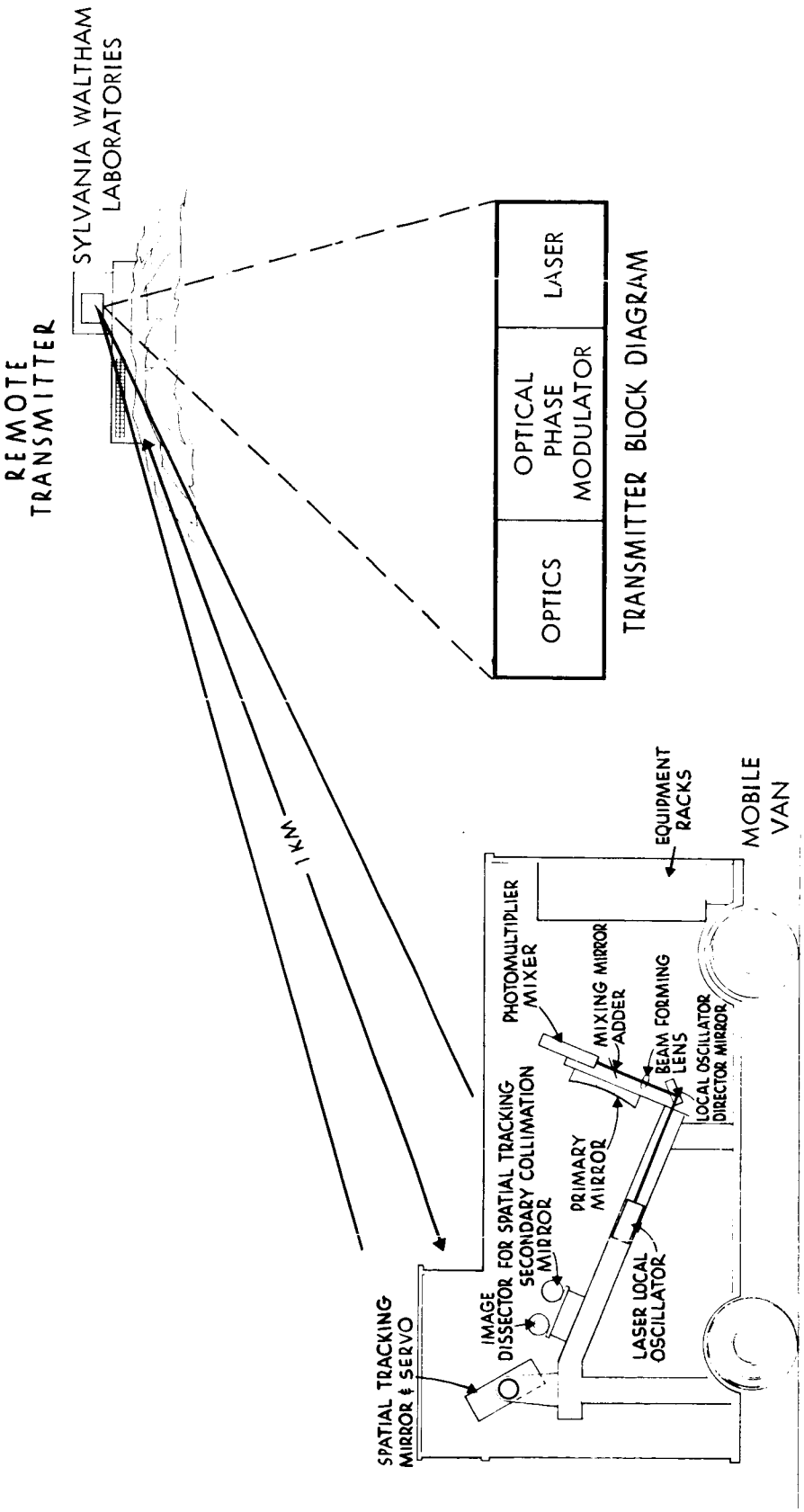

Figure 6. Coherent Laser Communications Experiments

modulated system, a coherent amplitude-modulated system, and a coherent frequency-modulated system. Both short- and long-term results have been obtained. In addition to performing experiments for the fixed 20.3 cm aperture of the receiver, the effect of varying the aperture size was determined for both coherent and noncoherent detection.

1.3.1 System Performance

The received signal power, P_s, at the photomixer is given by the expression

$$P_s = \frac{\epsilon_2 P_T D_c^2}{\theta^2 R^2} \tag{4}$$

where

ϵ_2 = receiver optics efficiency

P_T = transmitter power

D_c = optical collector diameter

θ = half-power transmitter beamwidth

R = distance between terminals

The heterodyne receiver operates in the photon noise-limited operation mode; thus, the voltage signal-to-noise ratio $\frac{e_{so}}{e_{no}}$ is given as:

$$\frac{e_{so}}{e_{no}} = \epsilon_1 \sqrt{\frac{P_s Q}{h\nu \Delta f}} \tag{5}$$

Typical system parameters are listed in Table 1 and the calculated results are listed in Table 2. The measuremnts were taken on a sunny morning when the air temperature was 75^{o} F and excessive turbulence was not noticeable.

TABLE 1

MEASURED EXPERIMENT PARAMETERS

Transmitter Power[a]	$P_T = 1.26\ 10^{-4}$ watts
Half-Power Transmitter Beamwidth	$\theta = 2 \times 10^{-3}$ radians
Range	R = 1 Km
Collector Aperture	$D_c = 0.2$ m
Measured Heterodyne Efficiency[b]	$\epsilon_1 = 4.5 \times 10^{-2}$ (rms)
Optical Efficiency	$\epsilon_2 = 2 \times 10^{-1}$
Quantum Efficiency[c]	$Q = 5 \times 10^{-2}$
IF Noise Bandwidth[d]	$\Delta f = 25$ MHz
Signal Power at Mixer[a]	$P_s = 4.2 \times 10^{-6}$ watts
Local Oscillator Power[a]	$P_R = 1.2 \times 10^{-5}$ watts
RMS Signal-to-Noise Ratio	$\frac{e_{so}}{e_{no}} = 17$ dB

(a) Measured with thermopile detector.

(b) Ratio of measured heterodyne signal voltage to calculated heterodyne signal voltage.

(c) Manufacturer's value.

(d) Corresponds to 8 MHz, 3-dB bandwidth.

TABLE 2

CALCULATED EXPERIMENT VALUES

Expected Signal Power at Mixer[a]	$P_s = 6.3 \times 10^{-6}$ watts
Expected Signal-to-Noise Ratio[a,b]	$\frac{e_{so}}{e_{no}} = 25$ dB

(a) Based upon measured transmitter power output.

(b) Based upon measured mixing efficiency.

The discrepancy between the calculated signal-to-noise ratio of Table 2 and the measured signal-to-noise ratio of Table 1 is apparently due to the excess noise observed from the laser local oscillator.

1.3.2 Fading Depth Data

A comparison of the fading characteristics during both noncoherent and coherent detection, using the optical superheterodyne receiver, is shown in Figure 7. The data is presented in the form of probability density functions for the fading signals. Thus, the probability of finding a signal in the voltage range $v + \Delta v$ is the integral of the curve over Δv. The curves, obtained by passing the analog signal voltage through a signal amplitude density analyzer, represent a 30-second period of data. The amplitude density sampling increment was allowed to scan through the signal fluctuations at a rate of 67-millivolts/second for the noncoherent data and 135-millivolts/second for the coherent data.

Although experiments have shown that the details of the density function do not remain stationary over the 30-second interval and minor distortions result in the analyzer because of time constant-sweeptime conflicts, it has been observed that the general curve shapes are representative. The fluctuations in the curves are probably produced when the distribution changes abruptly. The analyzer's decay time is longer than its rise time, thus producing noticeable exponential decay as the amplitude density suddenly decreases. The analyzer is calibrated by applying a sine wave of known amplitude at the input and thus reproducing the well-known density function for the sine wave on the paper recorder. This calibrated function then provides the scale factors for the unknown data inputs.

The received power signal voltage probability density functions are shown in Figure 7 for sunny-clear, overcast, and light rain conditions. The average received signal value is approximately in the center of the density function. Note that the minimum signal level, which occurs at the point where the amplitude density function starts to increase, is always appreciably greater than zero.

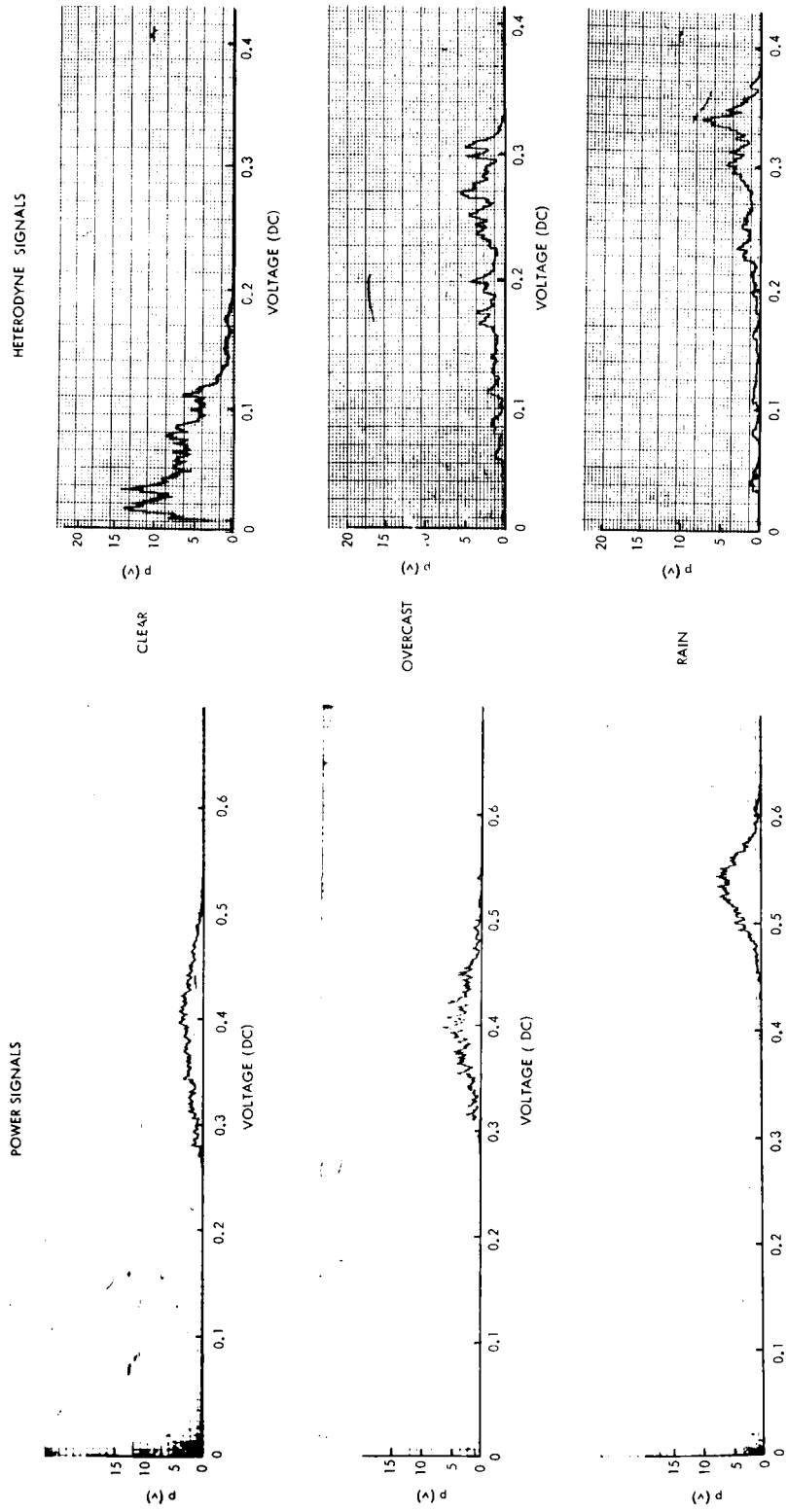

Figure 7. Comparison of Probability Density Functions for Signal Fading for Non-coherent and Coherent Optical Detection.

The decrease in fluctuation amplitude (i.e., the width of the distributions) indicates less turbulence on light rainy days as compared to clear days. These data reflect the fact that the thermal air gradients on rainy days are less than on sunny, clear days. The curves also imply greater beamwidth spreading on sunny, clear days because of the lower signal voltage. Our qualitative experience has been that as the rain increases, beamspreading will then increase also.

The corresponding heterodyne signal voltage density functions are shown also in Figure 7 for the same weather conditions. In each case the heterodyne signal is derived from the power signal by mixing the incoming power signal with the laser local oscillator. (The coherent and noncoherent detected signals are then separated by the intermediate frequency amplifier-filter.)

The heterodyne signal reflects not only signal power fluctuations but also phase fluctuations. The heterodyne signal is proportional to the square root of the power; thus, the heterodyne signal detection technique should smooth the power fluctuations. The large fading depths shown on a sunny, clear day indicate that the phase distortion on this day was quite severe and that the received wavefront probably was severely distorted.

On days when the atmospheric path apparently had fewer thermal gradients and thus had fewer turbulons, the heterodyne signal fading was less severe as shown also in Figure 7. The trend of reduced signal fluctuation with reduced turbulence is the same for both noncoherent and coherent detection. Table 3 shows the average mixing efficiency for each data sample.

Figure 8 is a record of the long-term signal fluctuations for both noncoherent and coherent detection. Data points representing an average value are recorded every 2 seconds. The entire record spans a period from 9:30 a.m. to 1:30 p.m. The downward trend in the power signal was found to be due to a transmitter steering effect caused by thermostructural changes at the transmitter. The heterodyne signal change was due to local oscillator-received misalignment, again due to thermostructural effects. These data were taken with the system air conditioner off and demonstrate the necessity of minimizing temperature changes. At the end of the four-hour span the mixing was realigned and the heterodyne signal level improved. Later the transmitter was

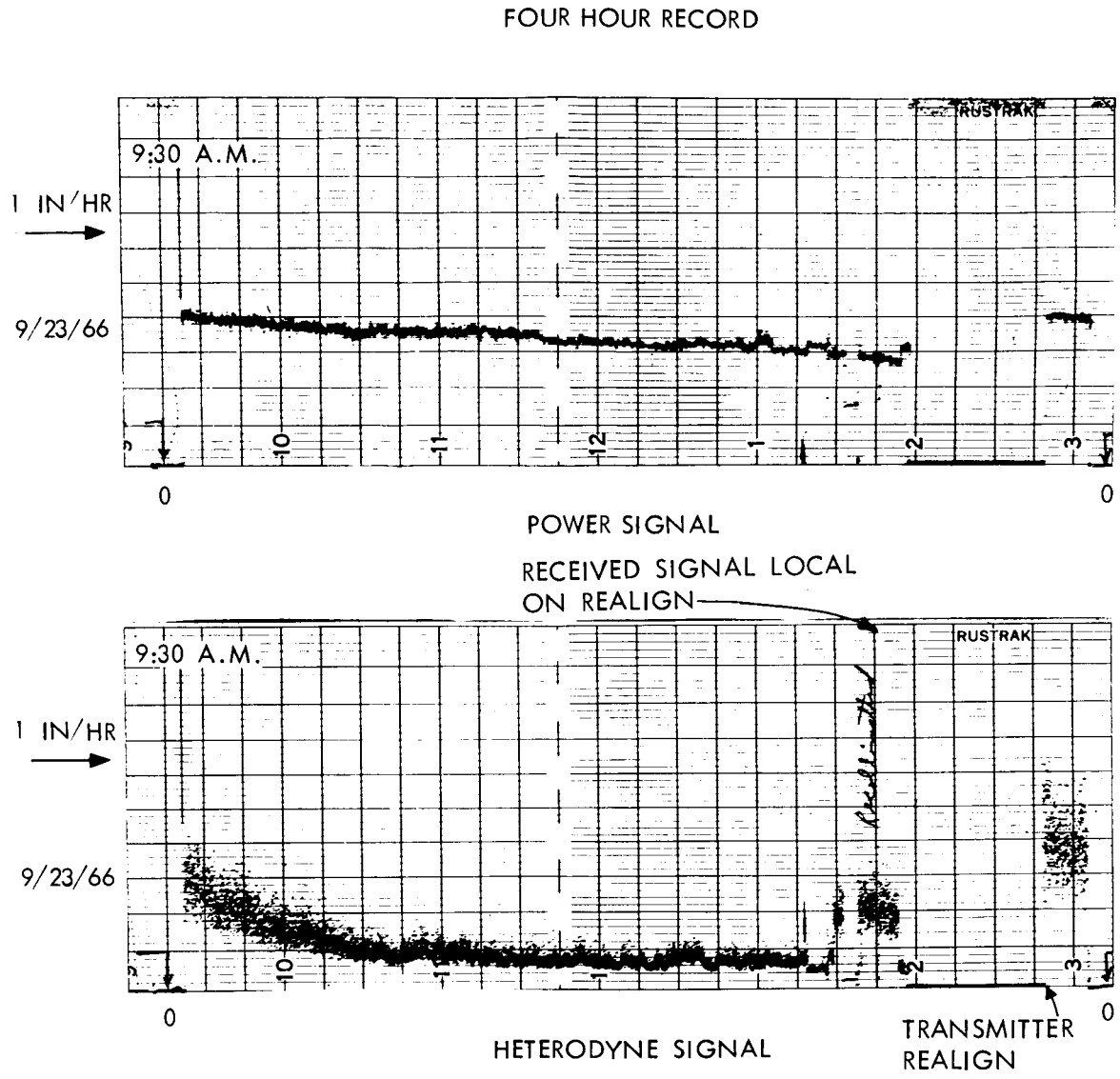

Figure 8. Long Term Fading of Non-coherent and Coherent Optical Detection in Optical Superheterodyne Receiver.

realigned and the original signal levels were restored. In general, when operating the van with a simple thermostat heat control, the mixing alignment can be easily retained. The greater fluctuation of the heterodyne signal, as compared to the received power signal, is evident. In general, our experiments in long-term fading effects, besides showing equipment instabilities, have shown that significant change in average path transmission occurs primarily when significant weather changes occur. In particular, (as expected) when fog, heavy rain, or snow occur, the average transmission decreases. To date we have been unable to detect any unexplainable long-term fading phenomenon.

1.3.3 Fading Rate Data

The frequency spectra of the fading signals are shown in Figure 9. It is significant to note that the heterodyne signals contain stronger higher frequency components than the corresponding power signals. These data again show the large influence of phase fluctuations along the atmospheric path on the heterodyne signal. The similarity of variations of the signal fluctuation frequency with weather for both detection techniques is apparent.

1.3.4 Frequency Modulation Experiment

At standard communication frequencies an advantage of FM over AM is that atmospheric disturbances will, in general, only affect the AM system. This occurs because the limiting and detection processes of FM discriminate against amplitude modulation components and thus recover the FM signal unaffected by atmospheric distortion. In addition, because of the nonlinear limiting process involved in FM systems as compared to an AM system, the fading characteristic should be different. The purpose of this experiment is to demonstrate this effect and compare the coherent FM method to the noncoherent AM and coherent AM methods.

In this experiment the single frequency transmitter laser was phase modulated at a 1-MHz rate with a modulation index (deviation ratio) of 0.5. For this value of modulation index the resultant modulation is classified as narrow-band FM, since only two carrier sidebands are produced. Figure 10 shows the signal spectrum as displayed on a spectrum analyzer.

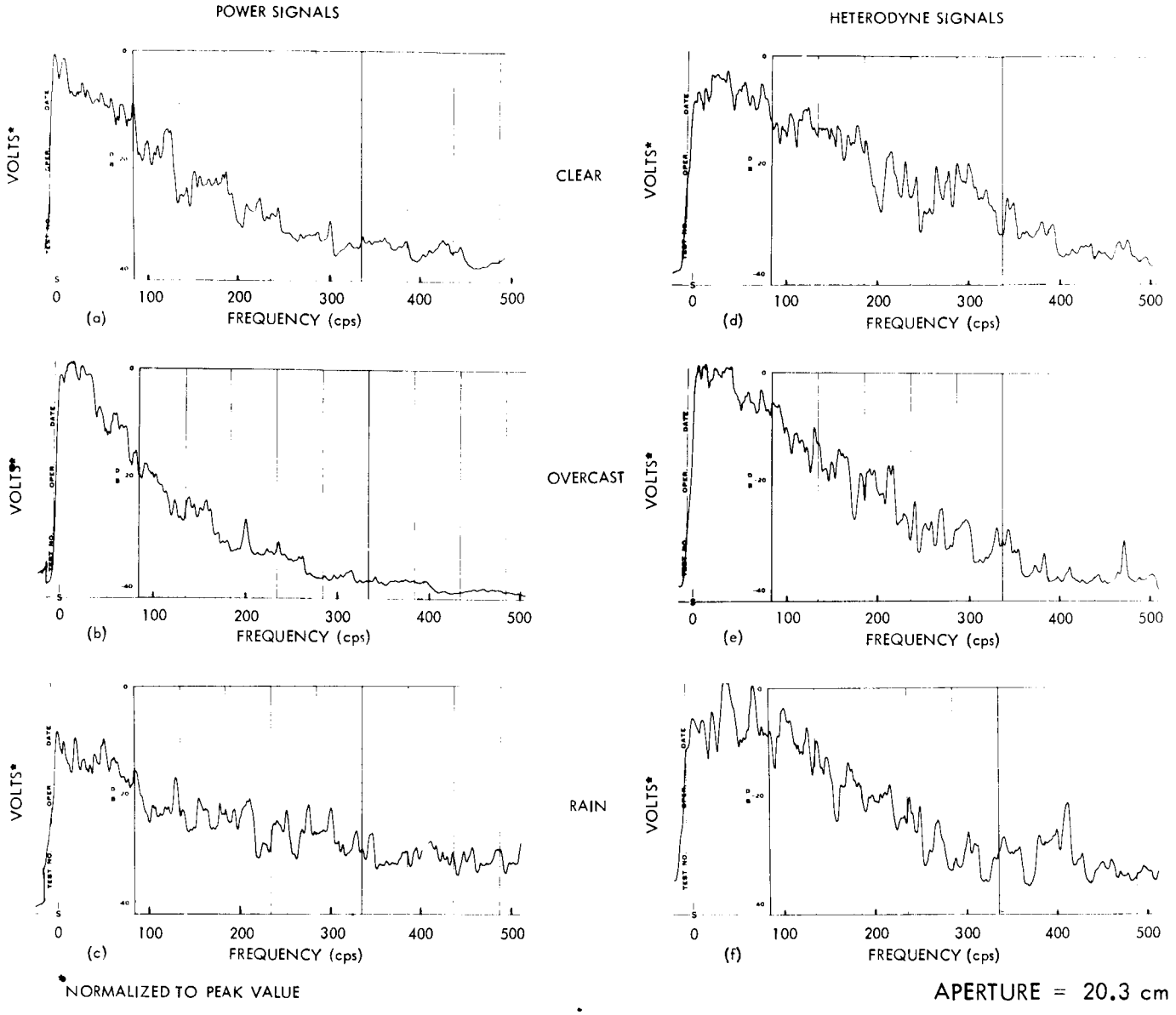

Figure 9. Comparison of Amplitude Fading Spectrum for Non-coherent Optical Detection.

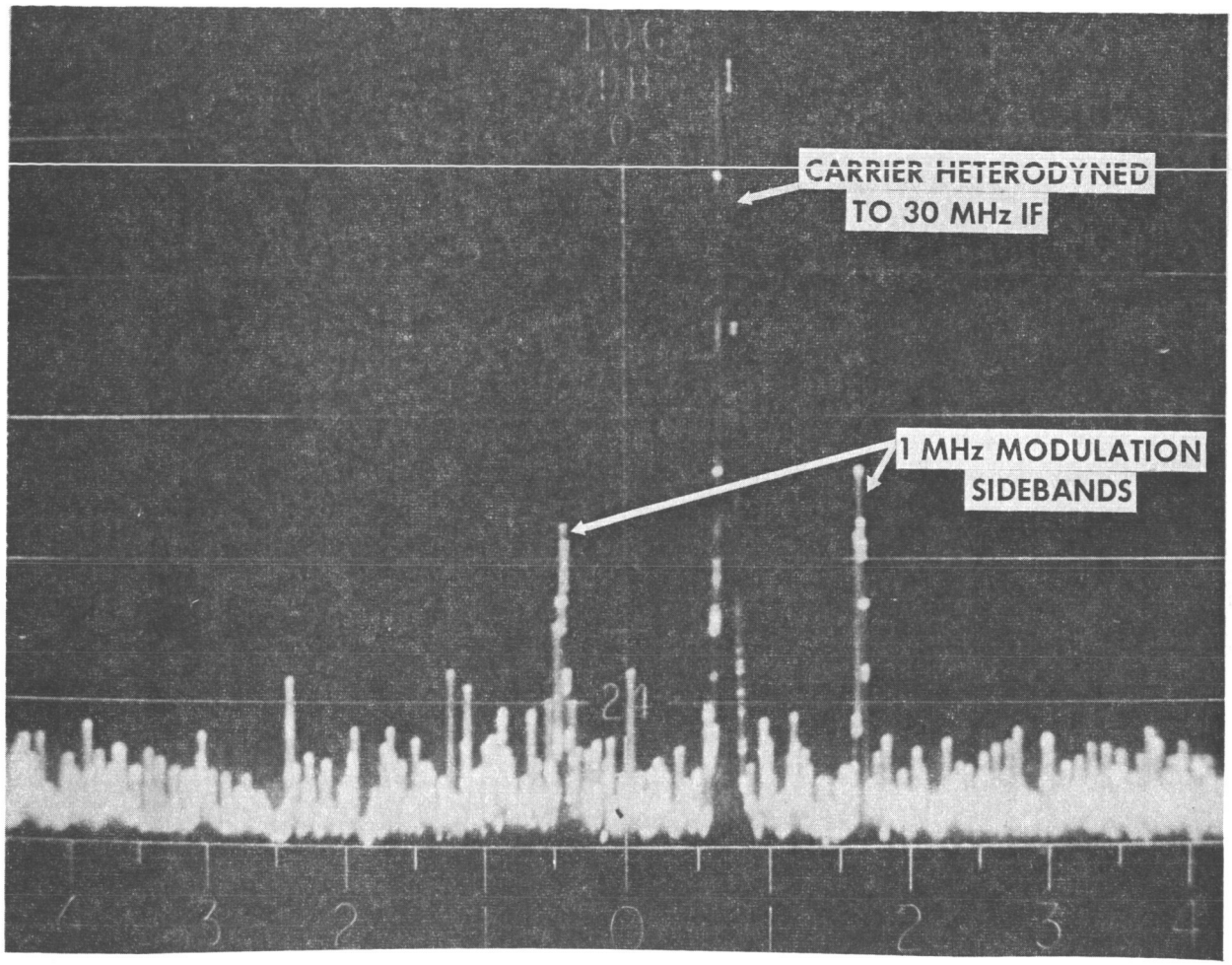

Figure 10. Spectrum of Frequency Modulated Laser Signal Propagated Over 1 KM Atmospheric Path and Received by Optical Superheterodyne Receiver.

Figure 11 shows the output of the discriminator of the FM channel of the optical superheterodyne receiver and demonstrates the nonlinear thresholding action of the limiter. When the receiver is not tuned in frequency to the incoming carrier, the discriminator output consists of only random noise. The major contributors to this noise is the power of the local oscillator. The combined noise produced by optical background radiation, photomixer dark current, and the thermal noise of the IF amplifier is less than that produced by the optical local oscillator power. When the receiver is tuned to accept the beat frequency with the signal from the remote laser transmitter, the noise output of the discriminator decreases and the 1-MHz frequency modulation shown in Figure 11 is observed. The thickness of the trace in the tuned case is caused by low-frequency microphonics which frequency-modulate the local oscillator. If the local oscillator were acoustically isolated, the observed noise level would then be the frequency jitter of the automatic frequency control system or phase modulation introduced by the atmosphere.

Whenever the signal fades, an increase of noise representing the untuned condition is observed. Because of the nonlinear action of the limiter only large fades are observable and the smaller fades are negligible. Oscillogram comparisons of the fading heterodyne signal with the discriminator output show this effect clearly. In addition, the amplitude modulation sidebands placed on the incoming signal by atmospheric turbulence are removed in the discriminator.

Using the present optical superheterodyne system, it has been observed that the optical FM system is analogous to a radio frequency FM system. In addition, frequency modulation of the optical carrier by the atmosphere has not been observed. We have thus concluded that the heterodyne signal fading characteristics of Figure 7, and a knowledge of the limiter-discriminator characteristic, are sufficient to quantitatively predict the performance of an optical frequency modulation system.

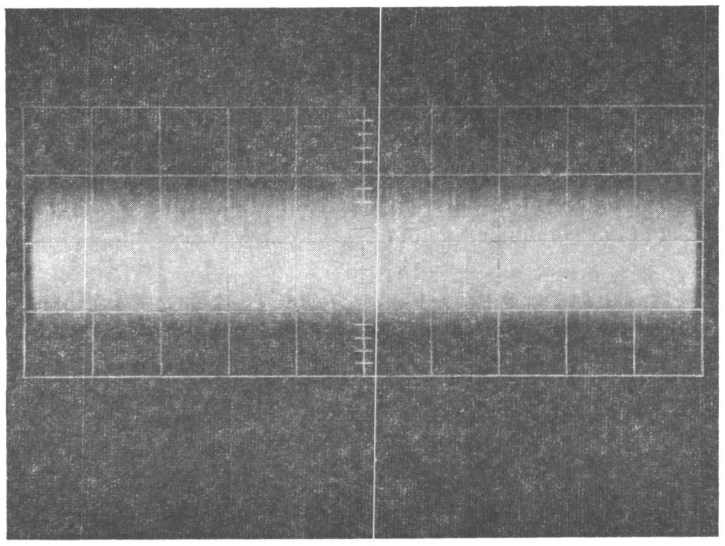

NOT TUNED

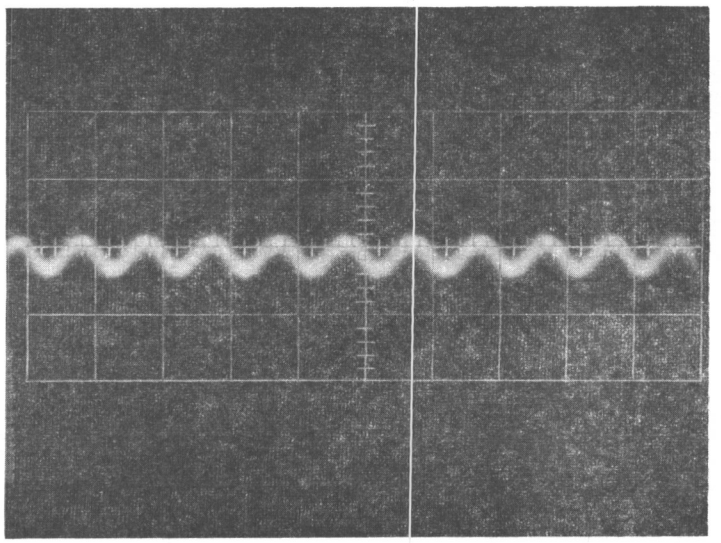

TUNED

Figure 11. Quieting Effect of FM Optical Superheterodyne Receiver Discriminator Output.

1.3.5 Effect of Aperture Size on Both Coherent and Noncoherent Detection

As the receiver collecting aperture is reduced, both the power signals and heterodyne signals would be expected to change their fading characteristics.[6-14] Data taken on a clear, sunny day and shown in Figure 12 shows the effect upon the power signal level and its amplitude fading density distribution as the aperture size is reduced. The aperture areas were reduced in steps of a factor of 2 and the corresponding average signal levels, located at the center of the density functions, also decreased approximately in the same ratio. The signal fluctuation can also be seen to increase with decreasing aperture. Figure 13 shows the effect observed on the heterodyne signals. The apparent jagged behavior of the density distribution is due to a rapidly changing distribution. (Long-term averaging of the distributions was beyond the capability of the density distribution analyzer.)

In making the measurements, the aperture stops were placed over the photomixer in order to limit the local oscillator signal only to the signal areas. The aperture dimensions reported have been referred to the input by multiplying by the focal length ratio. As the aperture is reduced, the mixing efficiency might be expected to improve.

Table 4 shows the measured mixing efficiencies and the corresponding input aperture. The data show that as the aperture size is reduced the mixing efficiency increases.

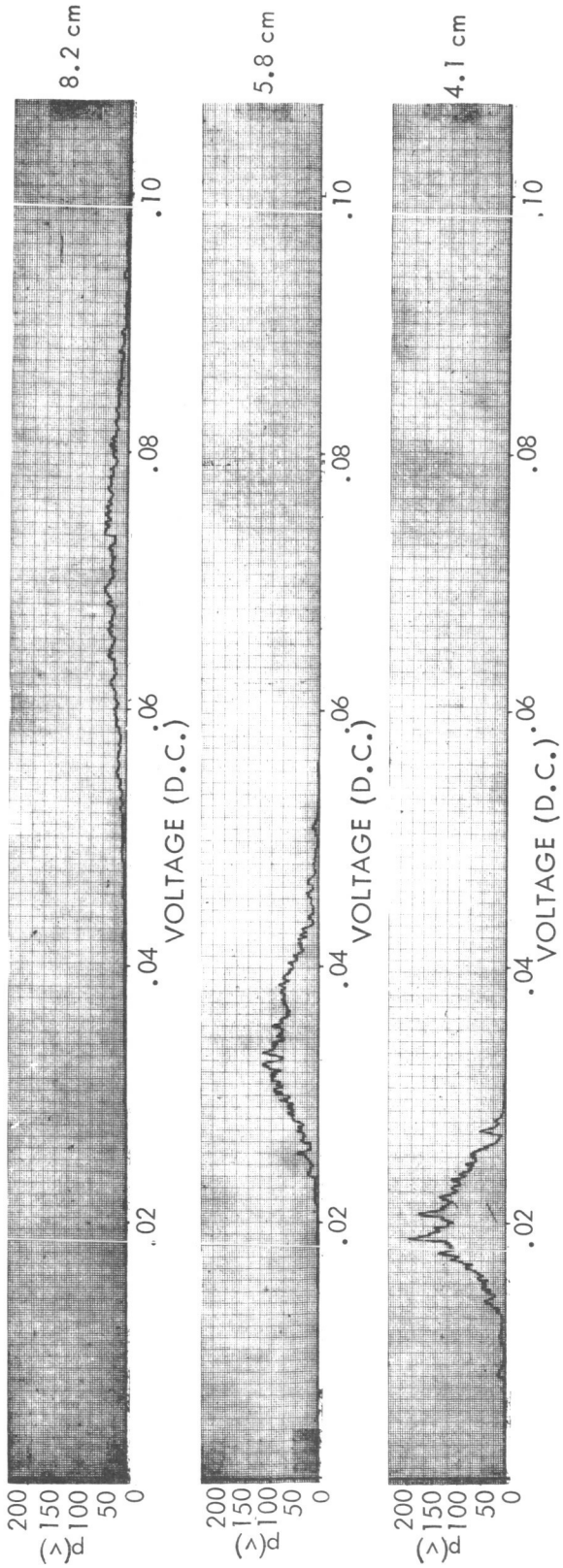

Figure 12. Dependence of Power on Aperture Diameter

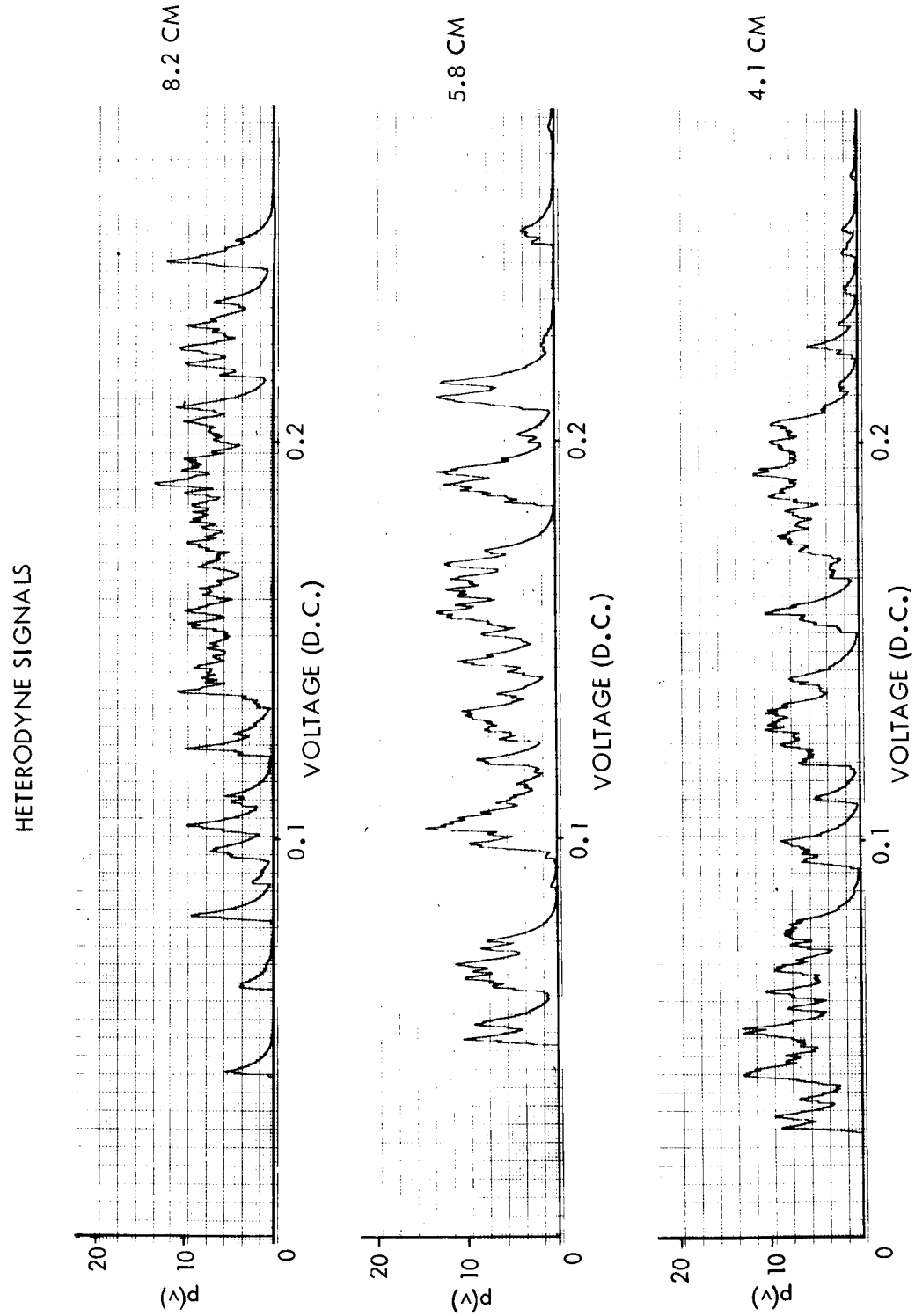

Figure 13. Dependence of Heterodyne Signals on Aperture Diameter

TABLE 3

HETERODYNE EFFICIENCY FOR VARIOUS WEATHER CONDITIONS WITH 20.3 CM APERTURE

Clear	1.79%
Overcast	3.45%
Rain	3.64%

TABLE 4

HETERODYNE EFFICIENCY FOR VARIOUS APERTURES

8.2 cm diameter	8.8%
5.8 cm diameter	13.7%
4.1 cm diameter	24.6%

PART 2

GROUND-TO-SPACE-TO-GROUND COMMUNICATIONS EXPERIMENT

2.1 INTRODUCTION

The purpose of this experiment was to passively acquire and then illuminate the retroreflector type satellite Explorer 22 with CW laser radiation and monitor the reflected intensity. The data collected would then be compared with starlight scintillation and ground-based laser propagation experiments. It was hoped that these initial measurements of scintillation, produced during a laser beam transport through the entire atmosphere, would yield data meaningful to space-to-ground laser communications applications. Our work indicated that the presently available CW laser power is inadequate. However, the experiment was carried to the point where the necessary improvements to perform the experiments are estimated to be 10^2 to 10^3 in order to cover the expected scintillation frequency range. In addition to this result, all the techniques of initial satellite acquisition and passive tracking have been developed and are applicable to using the optical superheterodyne receiver in future air-to-ground or space-to-ground experiments.

2.2 EXPERIMENT DESCRIPTION

The Sylvania Precision Laser Tracking System[2] was retrofitted to perform the experiment. The retrofitting included the installation of 1) a 80 mW, 0.25 milliradian beamwidth, He-Ne, 6328 Å laser; 2) a 5-inch diameter wide-field spotting telescope; 3) an auxiliary image dissector optical system to reduce the instantaneous field of view of 0.5 milliradians.*

Initially it was planned to operate solely from the tracking system and monitor the signal return from the image dissector. A series of laser back-

*It was experimentally found that the local atmospheric "breathing" effects precluded the use of smaller apertures. The skyglow measured with this field was approximately 100 times dark current level.

scatter measurements demonstrated the necessity of utilizing a remote receiver.

The final experiment approach is depicted in Figure 14. The tracking system was implemented with a stop-band filter that passed 50 percent of the incident solar reflected light from the Explorer 22 but attenuated by greater than 100 the wavelengths longer than 6000 $\mathring{A}$. Consequently, laser backscatter light would not affect the tracking unit. The experiment plan was to passively acquire and track the satellite while simultaneously pointing the laser beam at the satellite with the tracking mirror. A remote wide-field (2^{o}) receiver was to be manually pointed by an operator using a spotting scope. The remote receiver was located approximately 150 feet from the tracker in a direction such that the return signal, as determined from the Bradley effect, should be a maximum. The system outputs, including the image dissector signal and remote receiver, were recorded for future analysis. The experiment parameters are listed in Table 2-1.

The van location was surveyed by using the sun as a reference. The azimuth and elevation mirror angles were measured as a function of time while the system tracked the sun. Using "Air Almanac" data, the absolute pointing calibration was then determined. Precision data on the satellite's position were obtained weekly from the Smithsonian Astrophysics Observatory and transformed by computer into the tracking system coordinates. This procedure and the built-in accuracy of the equipment allowed the laser beam to be preset at a satellite's location to within 0.8 milliradians.

2.3 EXPERIMENTAL RESULTS

The experiments were performed at night during the period of March to August 1966. Much of the work involved a learning function prior to the final conclusive test. In May the Explorer 22 was successfully tracked passively by the tracking system. A strip chart record extracted from the magnetic tape recording of the image dissector signal is shown in Figure 15.

During this passive tracking experiment the satellite moved across the location of a star brighter than the satellite and caused the system to break lock.

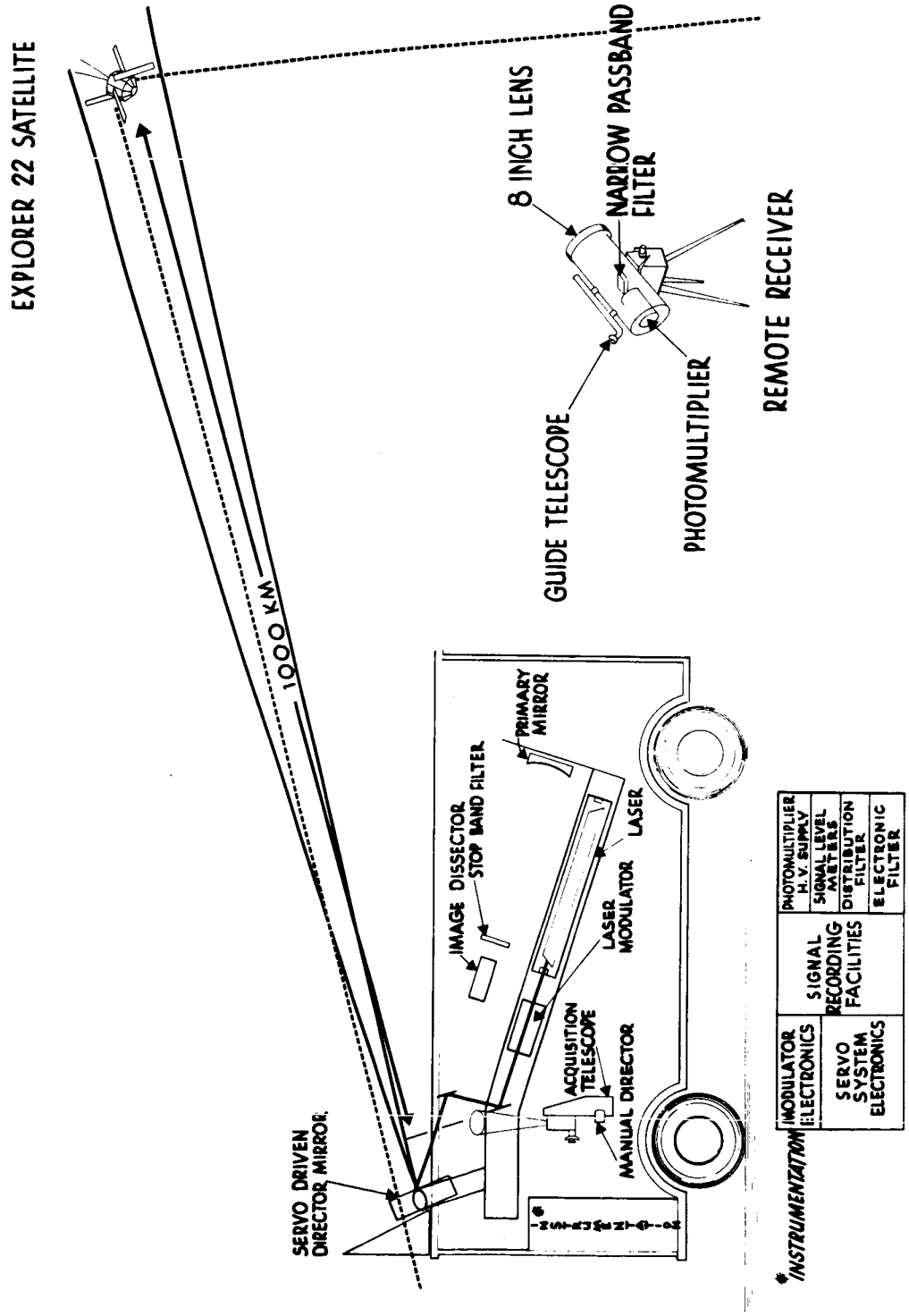

Figure 14. Explorer 22 Tracking Experiment

TABLE 2-1

GROUND-TO-SATELLITE-TO-GROUND LASER COMMUNICATION EXPERIMENT

Minimum Tracking System Passive Threshold in Local Skyglow Environment	+8.5 Visual Magnitude Star
Visual Magnitude Explorer 22	+7 to +8 Visual Magnitude Star
Laser Illuminator	80 mW, 0.25 milliradian beamwidth
Minimum Tracking System Accuracy	$\pm$25 microradian rms
Preset System Absolute Pointing Accuracy	0.8 milliradians
Operator-Observer Controlled Pointing Accuracy	$<$ 0.25 milliradian
Remote Receiver Minimum Detectable Flux Density	5×10^{-14} W/m^2
Calculated Laser Return Signal*	5×10^{-13} W/m^2 to 5×10^{-14} W/m^2

*Based upon private communication from H. Plotkin, (NASA - Goddard).

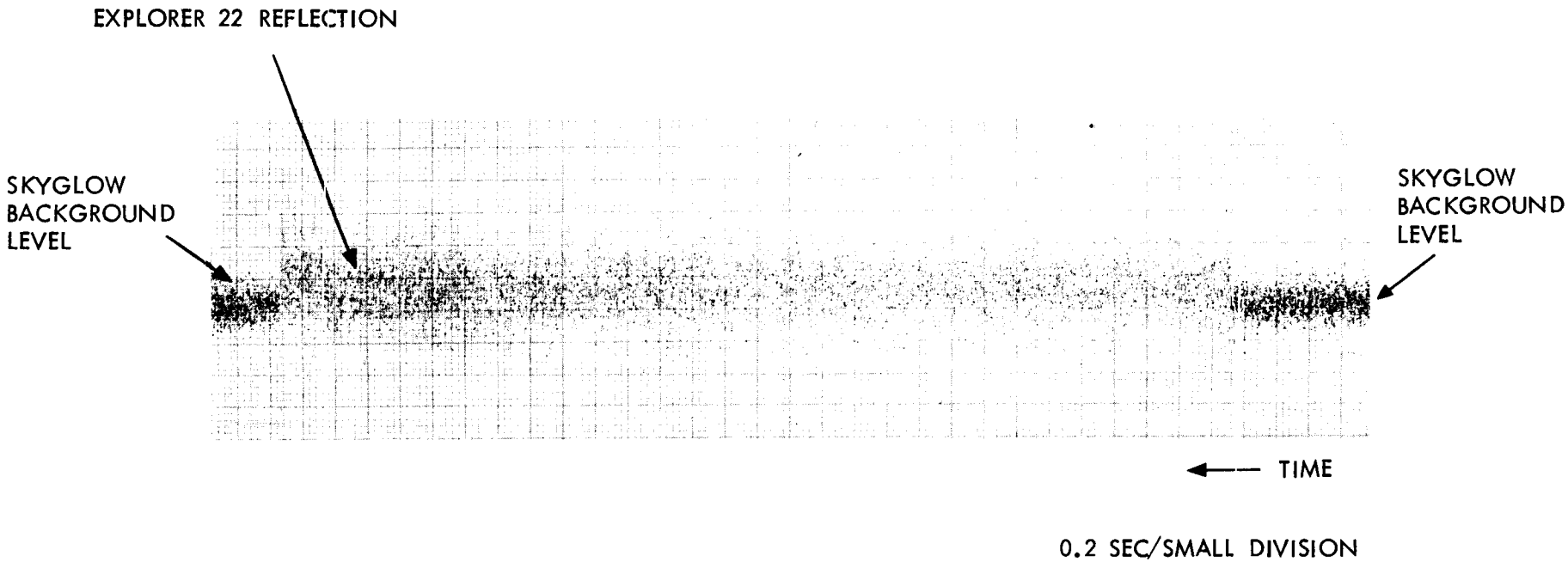

MAY 14, 1966 AT 1:28 A.M., EXPLORER 22 SIGNAL LEVEL EQUIVALENT TO + 7.0 VISUAL MAGNITUDE STAR.

SKYGLOW LEVEL EQUIVALENT TO +8.0 VISUAL MAGNITUDE STAR.

Figure 15. Passive Tracking Record of Explorer 22 Satellite

The satellite passes considered adequate for the experiment occurred during astronomical nighttime when the satellite was illuminated by the sun and at near zenith passes when the altitude ranged from 1000 km to 1500 km. Haze, clouds, weather, and excessive moonlight all produced interferences that hindered the experiment.

Approximately twenty-five satellite passes, ranging from two to five minutes in duration, were acceptable from March through August. Approximately 25 percent of these passes occurred when the weather, clouds, or haze did not interfere. On two of these nights satisfactory data were obtained. The first success, a passive track, has been described.

In the second success the satellite was observed but we were unable to track the satellite automatically. The reflected solar signal from the satellite corresponded approximately to a +8 visual magnitude star. The threshold of the tracking system limited by sky glow on this night was measured to be a visual magnitude between +7 and +8.

However, the trained operator was able to manually track and continuously point the boresighted 80 mW laser at the satellite over a period of about four minutes. The half-power beamwidth of the laser was 0.25 milliradians and the operator is able to manually control and point the system to an accuracy less than this beamwidth. During this period the operator of the wide field remote receiver, located at the position of anticipated maximum return, was able to continuously point this receiver at the moving satellite for a period of three minutes. The output of the remote receiver, which has a Minimum Detectable Flux Density of 5×10^{-14} W/m^2, as limited by dark current when equipped with a narrow-band 6328 Å filter at night, was recorded on tape.

Our calculations, based upon published data on the S66 and measurements made by H. Plotkin of NASA, indicated that the anticipated laser return would lie in a range of 5×10^{-13} W/m^2 to 5×10^{-14} W/m^2. The tape record, when examined with a four-cycle bandwidth amplifier centered around the laser modulation frequency, showed no return signal.

Based upon previous tests of the trained operator's pointing capabilities, we estimate that during the three-minute data collection interval several hits

must have been made, although the satellite may not have been continuously illuminated by the laser. Consequently, we concluded that the present system does not have the capability to perform the desired experiment, even in a narrow, electrical bandwidth. Thus, we discontinued these experiments.

If a meaningful communication experiment were to be performed, the system would have to be improved, by at least 40 to 60 dB. These improvements could be in the form of greater transmitter power, a larger collecting aperture, reduced skyglow, reduced aerosol backscatter, and possibly the application of cooled photomultipliers.

PART 3

AN IMMEDIATE APPLICATION OF THE OPTICAL SUPERHETERODYNE RECEIVER

This receiver is now ready to participate in space-to-ground communications experiments. For example, consider the Laser Communication Satellite Experiment (LCSE) proposed for the Apollo Applications Program. If a state-of-the-art 100 μW single frequency 6328 Å laser, similar to the present test transmitter source, were included in the satellite, an important coherent space-to-ground laser propagation experiment could be performed.

The LCSE experiment proposed by the Astrionics Laboratory of Marshall Space Flight Center will use a laser beam width of 2 microradians, and will be operated in a synchronous orbit at a distance of 34,000 km. Assuming a nominal atmospheric transmission of 50 percent, the flux density at the ground station would be approximately 1.4×10^{-8} W/m^2 if the spacecraft laser radiated 100 μW. This amount of power applied to the existing optical superheterodyne receiver will provide a 20-dB signal-to-noise ratio in a 500-Hz bandwidth. A 500-Hz bandwidth and 20-dB signal-to-noise ratio is adequate to obtain fading and fading-rate data for the propagation path.

In addition to the coherent data, noncoherent data may also be obtained for comparison, even during daytime hours. The ability to perform daytime noncoherent experiments reflects the precision-pointing accuracy of the angle tracking servo used to automatically align the receiver with the direction of the incoming laser beam.

Since the angle tracker has a peak-to-peak error of less than 100 microradians, a noncoherent receiver field of view can be limited to this value. The corresponding daylight blue sky level in a 2 Å interference filter bandwidth would be 3.2×10^{-11} W/m^2, which is much less than the predicted signal power density from the 100-μW laser. The signal-to-noise ratio in a 500-Hz bandwidth noncoherent receiver, using only 10 percent of the signal of the 20-cm heterodyne aperture, is approximately 30 dB.

Furthermore, if the LCSE laser illuminates the ground station, the optical superheterodyne can be operated completely independent of any other

facility. The manual acquisition techniques developed during Sylvania's Explorer 22 tracking experiments will permit the operator to acquire the spacecraft-borne laser. Once acquired, the angle tracking servo will automatically maintain the alignment between the receiver and the incoming beam, even if the satellite were moving at angular rates as high as 4 milliradians/second.

If the satellite is synchronous, the angular velocity will be considerably smaller. The automatic frequency control system of the superheterodyne receiver can operate over a 1-GHz range. The average Doppler shift anticipated for a synchronous satellite launched in a 60° orbit would be about 0.6 GHz. Thus, the coherent receiver can accommodate the expected Doppler shift.

PART 4

OPTICAL MODULATION CONSIDERATIONS

During the early phases of the present report period a study was performed to determine preferred transmitter modulation methods that could be utilized in optical communications experiments. The study was assisted by contributions from two other programs concerned with optical modulation methods. These programs included the Optical Technology Apollo Extension System (NAS-8-20256) and Sylvania's Independent Research and Development Program.

Pulsed, pulsed code, and direct modulation for both intensity and polarization modulation keying methods were evaluated for a continuous transmitter power output. It was found that pulsed code modulation using either intensity or polarization keying was significantly superior to the other methods. This study is presented as Appendix A.

A second study was performed to compare an intensity modulated optical communications system with frequency modulation of a carrier modulated intensity system. The results of this analysis, given in Appendix B, indicated that the system would have the usual advantage that a frequency modulated system has over an amplitude modulated system. This advantage lies in the fact that the limiting and discriminating process of FM detection provides a means of discrimination against amplitude noise modulation of the input signal, providing a minimum value of input signal to noise is maintained. In addition, the signal-to-noise power advantage of an FM carrier modulated intensity over a direct intensity modulated system is proportional to 1.5 times the square of the FM modulation index.

Consideration of a direct FM coherent system versus an AM coherent system indicated that this would be expected to be identical with the radio frequency case as discussed in Reference 2 of Appendix B.

A review of the modulation techniques studied indicated that before a particular system could be chosen in preference to another, greater knowledge of the transmission medium would be required. The knowledge required about the medium included fading depth, fading rate, and channel bandwidth for both

coherent and noncoherent detection techniques. In addition, the effect of varying both receiver and transmitter apertures on these systems is also required. Consequently, the experimental communication experiments concentrated upon obtaining fading depth and fading rate data for both the noncoherent and coherent detection techniques rather than prematurely testing modulation methods. In addition, a simple coherent frequency modulation experiment was performed to determine the comparative behavior of a radio frequency FM to optical frequency FM.

APPENDIX A

COMPARISON OF MODULATION TECHNIQUES FOR WIDE BANDWIDTH TRANSMISSION

by Dennis Gooding

A.1 INTRODUCTION

A study of modulation techniques was performed to determine an optimum form of modulation for a laser wide bandwidth link. The assumptions made for numerical comparisons of performance were that an output signal-to-noise power ratio of 30 dB is required and that the bandwidth is 5 MHz. The optical transmitter is limited in peak power capability rather than the average power capability. Background noise and photodetector noise are negligible compared to the quantum noise of the received signal and are neglected in the analysis here. In addition, for lack of better information, it is assumed that the power spectrum of the signal is constant over the frequency range -5 MHz to 5 MHz except for a DC component and zero elsewhere, and that the probability density function of the signal is uniform in the interval 0 to 1 and zero elsewhere.

The following kinds of modulation were considered:

(a) Pulsed intensity modulation

(b) Pulsed polarization modulation

(c) Direct intensity modulation

(d) Direct polarization modulation

(e) Pulse Code Modulation--intensity keying

(f) Pulse Code Modulation--polarization keying

A.2 RESULTS

Comparisons have been made strictly on the basis of an output signal-to-noise ratio, and no account has been taken of the relative subjective quality of the wide bandwidth (video) transmitted by analog and digital modulation

methods. Possibly, the output signal-to-noise ratios required to yield equal quality for analog and digital modulation techniques will be quite different. Furthermore, it seems likely that the relative subjective quality of these techniques will depend upon the particular use to be made of the wide bandwidth output. Table A-1 shows a comparison of R_o, the average number of received photons per second* at peak modulation required to obtain a 30-dB output signal-to-noise ratio for the various types of modulation listed and assuming a 5-MHz bandwidth.

TABLE A-1

COMPARISON OF MODULATION FORMS

Modulation	R_o (photons/second)	R_o (dB relative to PCM)
Pulsed Intensity Modulation	150×10^8	17
Pulsed Polarization Modulation	75×10^8	14
Direct Intensity Modulation	150×10^8	17
Direct Polarization Modulation	75×10^8	14
PCM--Intensity Keying	3.2×10^8	0
PCM--Polarization Keying	3.2×10^8	0
PCM--Polarization Keying with Error Correction Code	2.9×10^8	- 0.4

The results indicate that for a fixed output signal-to-noise ratio of 30 dB, the PCM modulation techniques will require substantially less peak transmitter output power than the analog techniques. On the other hand, a PCM system would be considerably more complex than an analog system and, because of the wider modulator bandwidth required, would require more modulator drive power than the analog system. These and other factors must be taken into account before a choice can be made between the various modulator systems considered herein. Only two of the assumptions made in the investigations are

*Only those photons which produce an output from the photodetector are considered, so detector efficiency does not enter into the results.

believed to critically affect the validity of the comparisons of the various systems. One is the assumption regarding the relative quality of analog and digital systems at equal output signal-to-noise ratios. The other is the assumption that an optical polarization analyzer can distinguish between two orthogonal states of polarization at extremely low photon arrival rates.

A.3 ANALYSIS

A.3.1 Pulsed Intensity Modulation

In the form of modulation considered here the signal X(t) is sampled at the Nyquist rate of 2W samples per second. Each sample is stretched (box-carred) to a duration of $\frac{1}{2W}$ seconds and intensity (power) modulates the optical carrier. Correspondingly, the photodetector converts light intensity into voltage pulses so that the overall transfer function of the modulator and demodulator is full-wave linear. The signal is recovered by averaging the received light intensity over each sample interval and putting the average, in the form of impulses each of whose strength is equal to its corresponding sample average, into a low-pass filter whose bandwidth is equal to the signal bandwidth. The model here is somewhat optimistic in that in practice one must sample at a rate slightly higher than the theoretical Nyquist rate in order to permit practical filters to be used. The error is negligible for the present purposes, however.

Let R_s be the average number of photons received during a sample interval when $\chi(t)$ takes on its largest value ($\chi = 1$). Assume that the gain of the photodetector is such that each photon produces a unit impulse of voltage. Let $z(t_n)$ be the number of photons received during the n^{th} sample interval. Then $z(t_n)$ is a Poisson random variable with average value $R_s\chi(t_n)$. The probability distribution of $z(t_n)$ is

$$P\left|z(t_n)\right| = \frac{e^{-R_s\chi(t_n)}\left|R_s\chi(t_n)\right|^k}{k!} \qquad \text{(A-1)}$$

and its variance is equal to its average value $R_s \chi(t_n)$. The output signal $\chi(t)$ is obtained by counting the number of photons received in the sample interval and dividing by R_s. That is,

$$\hat{\chi}(t_n) = \frac{z(t_n)}{R_s} \tag{A-2}$$

The expected value of error in $\hat{\chi}(t_n)$ is zero. The variance of the estimate, given $\chi(t_n)$, is

$$\text{var}\,(\hat{\chi}|\chi) = \frac{1}{R_s^2}\,\text{var}\; z = \frac{1}{R_s^2}\,(\chi R_s) \tag{A-3}$$

$$= \frac{\chi}{R_s}$$

The unconditional variance is found by averaging over all possible values of $\chi(t_n)$

$$\text{var}\,(\hat{\chi}) = \frac{1}{R_s}\int_o^1 \chi d\chi = \frac{1}{2R_s} \tag{A-4}$$

The signal power is

$$E\left|\chi^2(t_n)\right| = \int_o^1 \chi^2 d\chi = \frac{1}{3} \tag{A-5}$$

The signal-to-noise ratio of the reconstituted signal $\chi(t)$ is equal to the signal-to-noise ratio of its sample values $\chi(t_n)$, which is given by

$$\text{SNR} = \frac{E\left|\chi^2\right|}{\text{var}\left|\hat{\chi}\right|} = \frac{\frac{1}{3}}{\frac{1}{2R_s}} = \frac{2R_s}{3} \tag{A-6}$$

Finally, the required photon rate per second R_o is given by

$$R_o = (2W)R_s = \frac{3}{2}(2W)(SNR) \tag{A-7}$$

Taking $W = 5 \times 10^6$ and SNR = 1000, $R_o = 1.5 \times 10^{10}$ photons/second. (A-8)

A.3.2 Pulsed Polarization Modulation

This type of modulation differs from pulsed intensity modulation as described in the previous Section in that the stretched samples of the signal $\chi(t)$ are used to control the polarization of the optical carrier rather than the intensity of the optical carrier. The signal changes the relative amounts of energy transmitted in each of two orthogonal states of polarization. The two states of polarization could be right and left circular polarization or two orthogonal plane polarizations, for example.

Let $S_1(t_n)$ and $S_2(t_n)$ represent the intensity of the two polarization components of the optical carrier. Then,

$$S_1(t_n) = \left|1 - \chi(t_n)\right| S_s \tag{A-9}$$

$$S_2(t_n) = \chi(t_n)\, S_s \tag{A-10}$$

where S_s is the total transmitted energy per Nyquist sampling interval. Any nonlinearity of the polarization modulator is assumed to be compensated for by predistorting $\chi(t)$ to give a linear overall characteristic.

The receiver is assumed to contain a polarization analyzer and photodetector matched to each of the two states of polarization. Cross-talk between detectors is assumed negligible. Let $z_1(t_n)$ and $z_2(t_n)$ be the total number of photons detected by each of the two detectors during the n^{th} sample interval, and let R_s be the expected value of the sum of $z_1(t_n)$ and $z_2(t_n)$. Then $z_1(t_n)$ and $z_2(t_n)$ are independent Poisson random variables with expected values $\left|1 - \chi(t_n)\right|R_s$ and $\chi(t_n)R_s$, respectively.

The output samples are formed from z_1 and z_2 by the following operation

$$\hat{\chi}(t_n) = \frac{z_2(t_n) - z_1(t_n) + R_s}{2R_s} \tag{A-11}$$

The expected value of $\hat{\chi}(t_n)$ is $\hat{\chi}(t_n)$ so the expected value of the error is zero. The variance of $\hat{\chi}(t_n)$ is

$$\text{var}\,(\hat{\chi}) = \frac{1}{(2R_s)^2}\left|\text{var}(z_2) + \text{var}\,(z_1)\right|$$

$$= \frac{1}{(2R_s)^2}\left|\chi R_s + (1-\chi)R_s\right| \tag{A-12}$$

$$= \frac{1}{4R_s}$$

The expected value of $\chi^2(t_n)$ was found previously to be 1/3, so the signal-to-noise ratio is

$$\text{SNR} = \frac{4}{3} R_s \tag{A-13}$$

and

$$R_o = 2WR_s = \frac{3}{4}(2W)(\text{SNR}) \tag{A-14}$$

Taking $W = 5 \times 10^6$ Hz and SNR = 100 gives

$$R_o = 7.5 \times 10^9 \text{ photons/second} \tag{A-15}$$

A.3.3 Direct Intensity Modulation

In this case the signal is not sampled and boxcarred, but modulates the intensity of the transmitted light directly so that the average rate of photon emission is proportional to $\chi(t)$. The expected value of the rate of arrival of photons at the receiver likewise is proportional to $\chi(t)$. The receiver consists of a photodetector and a post-detection filter. The optimum filter and the performance of the system using that filter are found below.

The system can be modeled as shown in Figure A-1. The filter with frequency function $H(f)$ is chosen to minimize the mean-square error of the estimate of the time-varying part of the transmitted signal and rejects the constant part of the received signal. The mean value of $\chi(t)$ is assumed to be reinserted separately at the receiver. The process $R_1(t)$ is a sequence of unity impulses occurring at random with an average rate of $\chi(t)R_o$ impulses per second and represents the modulated photon carrier signal.

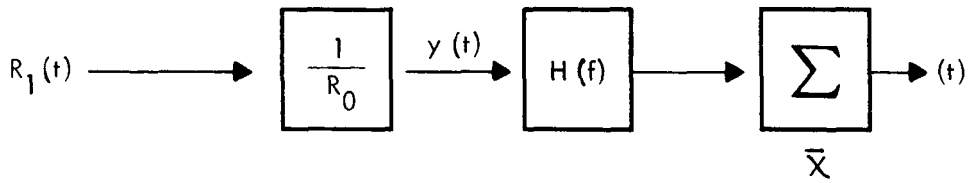

Figure A-1. Model of Direct Intensity Modulation System.

The optimum filter (not necessarily realizable) from the point of view of minimizing the expected value of $(\chi' - \hat{\chi}')^2$ is given by*

$$H(f) = \frac{S_{x'y}(f)}{S_y(f)} \qquad \text{(A-16)}$$

where $\chi'(t) = \chi(t) - \bar{\chi}$ is the time-varying part of $\chi(t)$, $S_y(f)$ is the power spectral density of the random process $y(t)$, and $S_{x'y}(f)$ is the cross-spectral density of $\chi'(t)$ and $y(t)$. The signal and $y(t)$ are assumed to be at least

*See, for example, Davenport and Root, Random Signals and Noise.

weakly stationary. The process y(t) can be regarded as a sequence of impulses of strength $\frac{1}{R_o}$ occurring randomly in time with an expected rate of $\chi(t)R_o$ impulses/second. In order to obtain $S_{x'y}(f)$ and $S_y(f)$, the corresponding correlation function $R_{x'y}(\tau)$ and $F_y(\tau)$ will be calculated. This is done by first regarding each impulse of y(t) as a finite pulse of width ϵ and height $\frac{1}{\epsilon R_o}$ and then letting ϵ tend to zero.

$$R_y(\tau) = E_x E_y\left\{y\left|\chi(t+\tau)\right| \, y\left|\chi(t)\right|\right\} \tag{A-17}$$

Two cases must be considered

A. $|\tau| > \epsilon$

$$R_{y\epsilon}(\tau) = E\left\{\left|\epsilon R_o \chi(t)\right| \, \left|\epsilon R_o \chi(t-\tau)\right| \left(\frac{1}{\epsilon R_o}\right)^2\right\}$$

$$= R_x(\tau) \tag{A-18}$$

B. $|\tau| \leq \epsilon$

$$R_{y\epsilon}(\tau) = E\left\{\left|\epsilon R_o \chi(t)\right| \left(\frac{1}{R_o^2}\right)^2 (1 - |\tau|)\right\} + R_x(\tau) \tag{A-19}$$

$$R_y(\tau) = \lim_{\epsilon \to 0} R_{y\epsilon}(\tau) = \frac{\bar{\chi}}{R_o}\delta(\tau) + R_\chi(\tau) \tag{A-20}$$

From cases A and B it can be seen that for all τ

$$R_y(\tau) = \frac{\bar{\chi}}{R_o}\delta(\tau) + R_x(\tau) \tag{A-21}$$

from which

$$S_y(f) = \frac{\bar{\chi}}{R_o} + S_x(f) = \frac{\bar{\chi}}{R_o} + \bar{\chi}^2\,\delta(f) + S'_x(f) \qquad \text{(A-22)}$$

The cross correlation $R_{x'y}(\tau)$ is given by

$$R_{x'y}(\tau) = E\left\{\left|\epsilon\chi'(t)\right|\left|\frac{1}{\epsilon}\,\chi\,(t+\tau)\right|\right\}$$

$$= R'_x(\tau) \qquad \text{(A-23)}$$

which gives

$$S_{x'y}(f) = S_{x'}(f) \qquad \text{(A-24)}$$

The optimum filter is, therefore,

$$H(f) = \frac{S_{x'}(f)}{\frac{\bar{\chi}}{R_s} + S_{x'}(f) + \bar{\chi}^2\,\delta(f)} \qquad \text{(A-25)}$$

If $S_{x'}(f)$ is a rectangular power spectrum of density $\frac{\sigma_x^2}{2W}$ between -W Hz and W Hz then H(f) is a rectangular frequency function between -W Hz and W Hz except for a zero at DC.

$$H(f) = \begin{cases} \dfrac{\sigma_x^2}{\frac{2W\bar{\chi}}{R_o} + \sigma_x^2 + 2W\bar{\chi}^2\,\delta(f)}, & |f| \le W \\ 0, & |f| > W \end{cases} \qquad \text{(A-26)}$$

This frequency function is not strictly realizable as a practical filter, but can be approximated quite well.

The output noise power is the mean-square difference between $\chi'(t)$ and $\hat{\chi}'(t)$ and if the optimum filter is used is given by*

$$N = \sigma_x^2 - \int_{-\infty}^{\infty} S_y(f)\, H(f)^2\, df$$

$$= \sigma_x^2 - \int_{-W}^{W} \frac{\frac{1}{2W}\,\sigma_x^4\, df}{\frac{2W\bar{\chi}}{R_o} + \sigma_x^2 + 2W\bar{\chi}^2\,\delta(f)}$$

$$= \sigma_x^2 - \frac{\sigma_x^4}{\frac{2W\bar{\chi}}{R_s} + \sigma_x^2}$$

$$= \frac{2W\bar{\chi}\,\sigma_x^2}{2W\bar{\chi} + R_o\,\sigma_x^2} \qquad \text{(A-27)}$$

The output signal-to-noise ratio is given by

$$SNR = \frac{\sigma_x^2 + \bar{\chi}^2}{N} = \frac{\sigma_x^2 + \bar{\chi}^2}{\sigma_x^2} + \frac{R_o\left(\sigma_x^2 + \bar{\chi}^2\right)}{2W\bar{\chi}} \qquad \text{(A-28)}$$

If the signal $\chi(t)$ is uniformly distributed between 0 and 1, $\sigma_x^2 = \frac{1}{12}$ and $\bar{\chi} = \frac{1}{2}$ giving

$$SNR = 4 + \frac{2}{3}\frac{R_o}{2W} \qquad \text{(A-29)}$$

*Davenport and Root, op. cit.

Solving for R_o, one obtains the final result

$$R_o = \frac{3}{2}(2W)(SNR-4) \approx \frac{3}{2}(2W)(SNR) \qquad (A-30)$$

For a high output signal-to-noise ratio, therefore, the required photon rates for direct intensity modulation and for pulsed intensity modulation are equal.

A.3.4 Direct Polarization Modulation

This form of modulation differs from pulsed polarization modulation in that the signal is not sampled and boxcarred but modulates the polarization of the optical carrier directly. The receiver continuously forms the quantity:

$$y(t) = \frac{z_2(y) - z_1(t) + R_o}{2R_o} \qquad (A-31)$$

and filters it with a filter having frequency function H(f) to obtain the best estimate of $\chi'(t)$, the time-varying part of $\chi(t)$. Here $z_1(t)$ and $z_2(t)$ are the output signals of two photodetectors, each of which is matched to one of the two polarization components of the received signal and is assumed to consist of a random sequence of unit impulses--one impulse for each detected photon. The quantity R_o is the average number of photons per second detected by both detectors.

The analysis of the optimum filter and the performance of this case is very similar to that for the case of direct AM and is omitted here. The optimum filter turns out to have the same frequency function (except for a gain constant) as for the direct AM case. The output signal-to-noise ratio and required photon rates are

$$SNR = 4 + \frac{4}{3}\frac{R_o}{2W} \qquad (A-32)$$

$$R_o = \frac{3}{4}(2W)(SNR-4) \approx \frac{3}{4}(2W)(SNR) \qquad (A-33)$$

The photon rate required for high values of the signal-to-noise ratio is approximately equal to that required in the case of pulsed polarizationmmodulation.

A.3.5 Pulse Code Modulation--Intensity Keying

In this case the signal is sampled at or above the Nyquist rate, quantized into $L = 2^M$ levels, and transmitted as a series of binary numbers by on-off keying the optical carrier. "On" is assumed to correspond to a binary 1 and "off" to a binary 6. The receiver contains a photodetector and other circuitry which determine whether or not at least one photon is received during a given binary digit (bit) interval. Since background radiation and dark current have been assumed negligibly small, an error in determining the identity of a given received bit will occur if and only if a binary 1 is transmitted and no photons are detected during the bit interval. When a binary 1 is transmitted the number of photons detected during the bit interval is a Poisson random variable with average value R_o, and the probability of detecting exactly n photons during the bit interval is

$$P(n) = \frac{e^{-R_b} R_b^n}{n!} \qquad \text{(A-34)}$$

If all L signal levels are equally likely, as assumed, then the PCM bits will take on the values 0 and 1 with equal probability. The probability of error P_b of an arbitrarily selected received bit is, therefore.

$$P_b = \frac{1}{2} P(0) = \frac{1}{2} e^{-R_b} \qquad \text{(A-35)}$$

In order to determine the required value of R_b it is necessary to assign an allowable value for P_b. Unfortunately, no data have been found which would indicate what bit error rate is required in a PCM system to give signal quality equal to that of an analog system operating at a given output signal-to-noise ratio. Lacking this information, it will be assumed, for purposes of prelimin-

ary comparison, that the quality of the two systems are equal when their output signal-to-noise ratios are equal.* In the case of PCM signal, the output noise consists of two parts, quantization noise and noise arising from bit errors.

The quantization noise power N_q is equal to the variance of the quantization error which for the assumed uniform distribution of $\chi(t)$ is

$$N_q = \frac{1}{12L^2} \tag{A-36}$$

In order to evaluate the noise N_b caused by bit transmission errors the receiver's estimate $\chi(t_n)$ of the n^{th} sample value of the signal $\chi(t)$ is written as

$$\hat{\chi}(t_n) = \sum_{k=0}^{M-1} \frac{1}{L} a_k 2^k \tag{A-37}$$

where a_k is the value, 0 or 1, of the k^{th} digit of the PCM word. Now, let $\epsilon(t_n)$ be the error $\chi(t_n) - \hat{\chi}(t_n)$ in the n^{th} sample. Then $\epsilon(t_n)$ can be expressed as

$$\epsilon(t_n) = \sum_{k=0}^{M-1} \frac{1}{L} a_k 2^k \tag{A-38}$$

where, since the a_k are equally likely to be 0 or 1, the probability distribution of c_k is

*This assumption has been made also by other investigators, including those responsible for Hughes Aircraft Company's Deep Space Optical Communications System Study.

$$P\,c_k = \begin{cases} \frac{1}{2} P_b\,, & c_k = 1,\ -1 \\ (1 - P_b), & c_k = 0 \end{cases} \qquad \text{(A-39)}$$

The occurrence of errors in the various bits is assumed to be independent.* Since the c_k have zero mean and are independent

$$N_b = \text{var}(\epsilon) = \sum_{k=0}^{M-1} \frac{1}{L}\, 2\, 4^k E\left[c_k^2\right]$$

$$= \frac{P_b}{L^2} \sum_{k=0}^{M-1} 4^k = \frac{\left(4^M - 1\right) P_b}{3L^2}$$

$$= \frac{\left(L^2 - 1\right) P_b}{3L^2} \qquad \text{(A-40)}$$

The total noise power N is the sum of N_q and N_b

$$N = \frac{1}{12L^2} + \frac{L^2 - 1}{3L^2} P_b \qquad \text{(A-41)}$$

and the signal-to-noise ratio is

$$\text{SNR} = \frac{E\left(X^2\right)}{N} = \frac{1/3}{N} = \frac{4L^2}{1 + 4\left(L^2 - 1\right)P_b} \approx \frac{4L^2}{1 + 4L^2 P_b} \qquad \text{(A-42)}$$

The error probability P_b depends upon L for any given value of R_s, the number of photons per sample, since

*This assumption is not a valid one if, for example, the signal undergoes slow fading.

$$R_b = \frac{R_s}{M} = \frac{R_s}{\log_2 L} \qquad \text{(A-43)}$$

Therefore, there exists an optimum value of L for each value of the signal-to-noise ratio which minimizes the required value of R_s. The last form of Equation (A-42) gives

$$P_b \approx \frac{1}{SNR} - \frac{1}{4L^2} \qquad \text{(A-44)}$$

A trial-and-error solution for SNR = 1000 gives the following optimum values for L, P_b, and R_b

$L = 32$ (5 bit PCM)

$P_b = 7.5 \times 10^{-4}$

$R_b = 6.4$ photons per bit

The required photon rate per second is

$$R_o = 6.4 \times 5 \times 10^7 = 3.2 \times 10^8 \text{ photons/second}$$

A.3.6 Pulse Code Modulation--Polarization Keying

This form of modulation is similar to PCM with intensity keying except that the PCM bits are transmitted as one of two orthogonal states of polarization of the optical carrier. The receiver contains a polarization analyzer and photodetector matched to each of the two states of polarization and makes bit decisions according to which detector responds to more photons during the bit transmission interval.

There is some uncertainty as to the amount of cross talk to be expected between the two photodetectors at low photon rates. It is not obvious whether or not a right circular polarization analyzer, for example, completely rejects

left circularly polarized light when the photon rate is very low. The cross talk will be assumed to be negligible for the present analysis. The analysis is easily modified to take cross talk into account.

Under the assumption of no background noise nor detector noise, a bit error can be made only if no photons are received by either photodetector, in which case an error will be made with probability 1/2 (assuming transmitted bits are equally likely to be 0 or 1). Let R_b be the expected number of photons received per bit. Then the probability of error per bit is, from Equation (A-34)

$$P_b = \frac{1}{2} e^{-R_b} \qquad \text{(A-45)}$$

as in the case of PCM with intensity keying. The analyses of the output signal-to-noise ratio and the required photon rate R_o apply to the present case, and the numerical results obtained hold also.

Therefore, the performance of PCM with intensity keying is equal to that of PCM with polarization keying under the conditions assumed. The performance of the latter can be improved slightly by employing a very simple error correction technique. A parity check bit would be appended to each PCM word, making a total word length of M + 1 bits. This would permit the receiver to fill in a single omission (failure to detect any photons with either photodetector) in a (M + 1)-bit word by choosing it two yield proper parity. Although no exact analysis of this technique has been made it is possible to estimate the effect of coding. First of all, if bit omissions are independent of each other the probability of exactly k omissions in an (M + 1)-bit word is

$$P_k = \binom{M+1}{k} P_{bo}^k \left(1 - P_{bo}\right)^{M-k+1} \qquad k = 1, 2, \ldots M+1 \qquad \text{(A-46)}$$

where P_{bo} is the probability of bit omission. If MP_{bo} is very small the probability of two omissions is large compared to the probability of more than two

omissions. Approximately, therefore, the probability P_e that errors will remain in the M information bits at the output of the error corrector is

$$P_e \frac{3}{4} P_2 = \frac{3(M+1)M}{8} P_{bo}^2 \qquad \text{(A-47)}$$

The factor of 3/4 arises because a probability of 1/4 exists that a random assignment of 0 or 1 to the two bit omission would be the correct one. As a further approximation, the error in a sample that results from two PCM bit errors is taken to be equal to that which would result from a single PCM bit error. This is a reasonable approximation since most of the sample error is contributed by the highest order bit in error. Therefore, P_e of Equation (A-47) can be substituted for P_b in Equation (A-44) to permit P_{bo} and, subsequently, the new value of R_o to be determined. Numerical evaluation for M = 5 gives

$$R_o = 2.9 \times 10^8 \text{ photons per second} \qquad \text{(A-48)}$$

This represents a 0.4 dB reduction compared to the system without error correction.

APPENDIX B

SIMPLE COMPARISON OF INTENSITY MODULATION VERSUS FREQUENCY MODULATION OF AN INTENSITY MODULATED SUBCARRIER TECHNIQUE FOR NON-COHERENT LASER COMMUNICATIONS

B.1 INTRODUCTION

An FM subcarrier optical receiver is shown in the block diagram of Figure B-1. In this receiver, the incoming wave consists of an optical signal whose intensity is modulated sinusoidally by a high-frequency carrier. The carrier itself is frequency modulated with the information signal. The optical signal is collected by the optics and focused through an optical filter onto the photomultiplier detector. The frequency-modulated subcarrier is detected by the photomultiplier that responds linearly to the intensity variations of the optical signal.

The signal now is a conventional frequency-modulated wave and can either be amplified or converted to another frequency. The intermediate-frequency amplifier in the conventional receiver would correspond to the bandpass amplifier of Figure B-1. In addition, the limiter, discriminator, and low-pass filter are also conventional. Random fluctuations (shot noise) in the phototube current are the predominant* noise source in the system of Figure B-1. The signal radiation photon noise, background photon noise, and the shot noise of the photomultiplier dark current all contribute to this current.

When a noncoherent optical receiver operates with this type of noise as a limit of sensitivity, it is operating optimally.[1] The large noiseless gain available with a photomultiplier allows the system to be designed for this limit. Thus, the noise that will limit an FM subcarrier optical receiver should be the shot noise in the photocurrent.

*Another noise source is the low-frequency optical signal scintillation produced as the signal is propagated along a turbulent atmospheric path containing parcels of air of varying index of refraction. This will be neglected in this discussion, because they can be removed by automatic gain control methods.

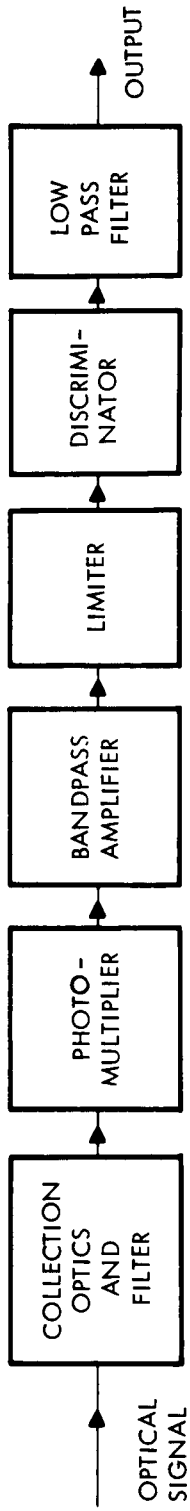

Figure B-1. Frequency Modulated Subcarrier Optical System.

B.2 SIGNAL ANALYSIS

For single frequency fm, the output signal e_s from the photomultiplier is

$$e_s = \frac{G_{pm}\rho P_s R_L}{2} \cos\left(\omega_c t + \beta \sin \omega_m t\right) \qquad \text{(B-1)}$$

where

G_{pm} = the gain of the photomultiplier

ρ = responsivity of photo-cathode

P_s = optical signal power (peak to peak)

R_L = photomultiplier load resistor

ω_c = subcarrier circular frequency $\left(\omega_c = 2\pi f_c\right)$

$\beta = \frac{\Delta\omega_d}{\omega_m}$ = modulation index

$\Delta\omega_d$ = maximum circular frequency deviation

ω_m = circular modulation frequency

After further amplification by the bandpass amplifier and subsequent limiting, the signal enters the discriminator. The discriminator output e_{so} is proportional to the instantaneous frequency deviation from the carrier frequency. Thus,

$$e_{so} = b\left(\omega - \omega_c\right) \qquad \text{(B-2)}$$

where

b = discriminator constant in volts/radian

ω = instantaneous circular frequency

Now

$$\omega = \frac{d}{dt}\left(\omega_c t + \beta \sin \omega_m t\right) \tag{B-3}$$

and thus

$$\omega = \omega_c + \Delta\omega \cos \omega_m t \tag{B-4}$$

Substituting Equation (B-4) into Equation (B-2) yields

$$e_{so} = b\Delta\omega_d \cos \omega_m t \tag{B-5}$$

and the mean signal power S_o in a 1-ohm resistor is

$$S_o = \frac{b^2 \Delta\omega_d^2}{2} \tag{B-6}$$

B.3 NOISE ANALYSIS

The mean square shot noise spectral density η at the output of the photomultiplier is:[1]

$$\eta = 2eG_{pm}^2 R_L^2 \left(\rho P_s + \rho P_B + I_D\right) \tag{B-7}$$

where

e = electronic charge

P_B = optical background power passing through optical filter

I_D = photo-cathode dark current

Applying the simplified analysis used by Schwartz,[2] if we assume the noise is represented by a discrete number of sine waves spaced by a frequency $\Delta\omega/2\pi$ and each wave having a mean square voltage of $\eta\Delta\omega/2\pi$, then the noise component at a frequency $\omega_c + \beta \sin \omega_m t + \omega$ is

$$e_n = \left(\frac{\eta\Delta\omega}{\pi}\right)^{1/2} \cos\left(\omega_c t + \beta \sin \omega_m t + \omega t\right) \tag{B-8}$$

Then adding the noise of Equation (B-8) to the signal given by Equation (B-1) results in

$$e_s + e_n = \left[\left(e_s\right)_{max}^2 + 2\left(e_s\right)_{max}\left(e_n\right)_{max} \cos \omega t + \left(e_n\right)_{max}^2\right]^{1/2} \cdot \cos\left(\omega_c t + \beta \sin \omega_n t + \theta\right) \tag{B-9}$$

where

$$\theta = \frac{\left(e_n\right)_{max} \sin \omega t}{\left(e_s\right)_{max} + \left(e_n\right)_{max} \cos \omega t} \tag{B-10}$$

where

$$\left(e_s\right)_{max} = \frac{G_{pm}\rho I_s R_L}{2} \tag{B-11}$$

and

$$\left(e_n\right)_{max} = \left(\frac{\eta\Delta\omega}{\pi}\right)^{1/2} \tag{B-12}$$

If

$$\frac{\left(e_s\right)_{max}}{\left(e_n\right)_{max}} \gg 1 \tag{B-13}$$

then

$$\theta \approx \frac{(e_n)_{max} \sin \omega t}{(e_s)_{max}} \qquad \text{(B-14)}$$

The limiter removes the amplitude modulation due to the noise. The noise output of the discriminator e_{no} is

$$e_{no} = b \frac{d\theta}{dt} \qquad \text{(B-15)}$$

$$e_{no} = b\omega \frac{(e_n)_{max}}{(e_s)_{max}} \cos \omega t \qquad \text{(B-16)}$$

The mean square noise voltage contribution at one frequency is

$$\overline{e}^2_{no} = \frac{b^2 \omega^2 (e_n)^2_{max}}{2(e_s)^2_{max}} \qquad \text{(B-17)}$$

substituting for $(e_n)_{max}$ in Equation (B-17) gives

$$\overline{e}^2_{no} = \frac{b^2 \omega^2 \eta \Delta\omega}{2(e_s)^2_{max}} \qquad \text{(B-18)}$$

If the low-pass filter is adjusted to pass frequencies up to f_m, the total noise power in the filter bandwidth is obtained by integrating all the $\Delta\omega$ contributions in Equations (B-18) from $-\omega_m/2\pi$ to $+\omega_m/2\pi$. Performing this operation gives the following value for the noise power N_o in a 1-ohm resistor.

$$N_o = \frac{\eta}{3\pi} \frac{b^2}{(e_s)^2_{max}} \omega_m^3 \qquad \text{(B-19)}$$

B.4 SIGNAL-TO-NOISE RATIO

The mean signal power to noise power ratio using Equations (B-6) and (B-19) and substituting β for $\Delta\omega/\omega_m$ yields

$$\frac{S_o}{N_o} = \frac{3\beta^2 (e_s)^2_{max}}{4\eta f_m} \tag{B-20}$$

Substituting for $(e_s)_{max}$ and η gives

$$\frac{S_o}{N_o} = \frac{3\beta^2 \rho^2 P_s^2}{32\ e f_m (\rho P_s + \rho P_B + I_D)} \tag{B-21}$$

as the signal-to-noise ratio for the FM system. Equation (B-21) holds only when the signal-to-noise ratio at the input to the limiter is large. The mean signal-to-noise ratio at this point may be obtained by taking the mean square value of Equation (B-1) and dividing it by the mean square noise of Equation (B-7) in the bandpass amplifier bandwidth Δf_a. The result is given by Equation (B-22).

$$\left[\frac{S_o}{N_o}\right]_{input} = \frac{\rho^2 P_s^2}{16\ e \Delta f_a (\rho P_s + \rho P_B + I_D)}$$

and the relationship between the output signal-to-noise and input signal-to-noise is

$$\left[\frac{S_o}{N_o}\right]_{output} = \frac{3}{2}\beta^2 \left(\frac{\Delta f_a}{f_m}\right) \left[\frac{S_o}{N_o}\right]_{input} \tag{B-23}$$

For a corresponding amplitude modulated receiver as compared to a frequency-modulated receiver the ratio of Equation (B-2) to Equation (B-22) for $f_m = \Delta f_a$ shows the relative performance to be

$$\left[\frac{S_o}{N_o}\right]_{FM} = \frac{3}{2}\beta^2\left[\frac{S_o}{N_o}\right]_{AM} \qquad \text{(B-24)}$$

Note that in order to get an improvement in performance using FM the modulation index must satisfy the relation

$$\beta \geq 0.82 \qquad \text{(B-25)}$$

B.5 REFERENCES CITED IN APPENDIX B

1. G. Biernson and R. F. Lucy, "Requirements of a Coherent Laser Pulse Doppler Radar," Proc. IEEE, vol. 51, no. 1; January 1963.

2. M. Schwartz, Information Transmission Modulation and Noise, McGraw-Hill Book Co., New York, 1959, p. 300.